NUMERICAL STUDY ON CYCLIC SEISMIC RESPONSES OF UNREINFORCED MASONRY WALLS RETROFITTED WITH LOW-STRENGTH ENGINEERED CEMENTITIOUS COMPOSITES

Master Thesis

Laura Kuandyk

School of Engineering and Digital Sciences

Department of Civil & Environmental Engineering

Nazarbayev University

53 Kabanbay Batyr Avenue, Astana, Kazakhstan, 010000

Supervisors: Dichuan Zhang, Chang Shon

Date of completion: April, 2024

Declaration

I hereby, declare that this manuscript, entitled “Numerical Study on Cyclic Seismic Responses of Unreinforced Masonry Walls Retrofitted with Low Strength Engineered Cementitious Composite”, is the result of my own work except for quotations and citations which have been duly acknowledged.

I also declare that, to the best of my knowledge and belief, it has not been previously or concurrently submitted, in whole or in part, for any other degree or diploma at Nazarbayev University or any other national or international institution.

Name: Laura Kuandyk

Date: 15.03.2023

Abstract

Most of the faults of Tien Shan Mountain are situated in Central Asia. Even the small faults of the mountain may cause risk to the nearby cities, such as Almaty, Kazakhstan, with a population of about 1.8 million people. Over half of the buildings in Almaty are unreinforced masonry buildings, followed by reinforced masonry, confined masonry, and reinforced concrete, and a minority of structures are from wood and steel. Unreinforced masonry buildings may demonstrate brittle behavior under seismic activities. Earthquakes such as those happened in the past of Almaty can damage most of the city and its inhabitants. The catastrophic destruction action of the earthquake can be mitigated by the construction of high strength, and ductile buildings, which can withstand large deformations with minor damages. Thus, to improve the response of existing unreinforced masonry structure, different studies propose the use a retrofitting, which can increase the deformation capacity and ductility of the unreinforced masonry walls. This thesis focuses on parametric study on cyclic responses of unreinforced masonry walls retrofitted with low-strength Engineered Cementitious Composite (ECC). The new retrofitting material, Engineered Cementitious Composite (ECC) with a high tensile strain hardening rate, was retrofitted to the unreinforced masonry wall in this study. Previous experimental studies have shown that the normal strength ECC can increase the strength of URM but has little effect on the deformation capacity due to the incompatibility of the masonry and composite. Moreover, a numerical study by Sailauova (2022) has shown that the low-strength ECC can increase the deformation capacity under monotonic loading because of stiffness compatibility between the masonry wall and composite. Considering the prior studies, this study addresses to the cyclic response of the masonry wall since the earthquake has a cyclic nature. The application of low-strength ECC approved the hypothesis that it can reach more deformation rather than normal-strength ECC, since it matches the stiffness of the masonry wall resulting in more ductile behavior.

This study aims to investigate the cyclic response of unreinforced masonry walls subjected to cyclic seismic loadings. This thesis presents a numerical study on in-plane cyclic behaviors of the unreinforced masonry wall retrofitted with the low-strength ECC. The numerical study was conducted on nonlinear two-dimensional models in ABAQUS software using a simplified micro-modeling approach for the masonry wall and the concrete damage plasticity for the ECC. The dynamic analysis using explicit analysis technique was adopted due to the non-linear behaviors of

the masonry wall and ECC. The model was verified from an existing experimental study. The study parameters include the strength of ECC, wall aspect ratios, and vertical pressures, which represent typical wall geometry and gravity loading conditions of unreinforced masonry buildings in Almaty. This study concentrates on 0.5, 0.75, and 1.0 wall aspect ratios and walls subjected to 0.43, 0.60, and 0.78 MPa vertical pressures, or in axial force ratio 0.10, 0.15 and 0.19, respectively. Moreover, the proposed material, Engineered Cementitious Composite (ECC), with different compressive strengths (10, 20, 30, 40, and 50 MPa) was evaluated. The behavior of the retrofitted wall under the cyclic loading was compared to that under the pushover analysis.

The numerical study results concluded that with the increase of ECC compressive strength on the retrofitted masonry wall, deformation capacity and ductility decrease, while wall strength and stiffness increases simultaneously. However, as the ECC becomes stronger, energy dissipation decreases. The effect of ECC for different wall aspect ratios on wall strength decreases with the increasing aspect ratio, but increases with the increase of vertical pressure. This is because the friction between the brick units and mortar increases. Regardless of the aspect ratio and vertical pressure, low strength ECC with compressive strength 10 and 20 MPa improve the lateral deformation capacity of the masonry wall. Moreover, the pushover analysis shows a slower strength reduction than the cyclic loading analysis due to the cumulative damage from the cyclic loading.

Acknowledgments

I would like to express my greatest gratitude to my research supervisor Professor Dichuan Zhang, who has constantly supported me throughout the journey of completing this master's thesis. I am deeply thankful for his encouragement, guidance, and expertise.

I also want to thank my co-supervisor, Professor Chang Shon, for his constructive feedback and comments on enhancing my master's thesis.

I am also thankful to my friends and colleagues for their encouragement, help, and motivation.

Finally, special gratitude goes to my family members for their continuous encouragement, support, and unconditional love.

Table of Contents

List of Symbols

E_w	Adjusted elastic modulus of wall brick (MPa)
E_m	Elastic modulus of mortar (MPa)
E_b	Elastic modulus of brick (MPa)
F_{cr}	Cracking strength (kN)
F_i	Lateral load at loop i (kN)
F_{max}	Maximum lateral load (kN)
F_u	Ultimate strength (kN)
G_{IC}	Mode I critical fracture energy in the axial direction (N/mm)
G_{IIC}	Mode II critical fracture energy in shear direction (N/mm)
H	Height of the wall (mm)
K_c	Ratio of the tensile to the compressive meridian or shape factor
K_i	Stiffness of the wall (N/mm)
K_{nn}	Stiffness of joint interface in the normal direction (N/mm^3)
K_{ss}	Stiffness of joint interface in shear direction (N/mm^3)
L	Length of the wall (mm)
f_w	Adjusted compressive strength of wall brick (MPa)
f_b	Compressive strength of the brick (MPa)
f_{b0}	Initial biaxial compressive strength (MPa)
f_{c0}	Initial uniaxial compressive strength (MPa)
f_m	Compressive strength of mortar (MPa)
h_b	Height of the brick (mm)
h_m	Mortar thickness (mm)
n	Number of vertical brick layers
t_n^{max}	Tensile strength of the joint interface (MPa)
t_s^{max}	Shear strength of the joint interface (MPa)
Δ_{cr}	Cracking displacement (mm)
Δ_{Fmax}	Deformation capacity at peak strength (mm)
Δ_i	Displacement at loop i, corresponding to F_i (mm)
Δ_u	Deformation capacity (mm)

ε	Eccentricity
ε_0	Compressive strain at peak stress
ε_r	Compressive residual stain
ε_t	Tensile ultimate strain
ε_{tp}	Tensile strain at peak stress
ε_u	Compressive ultimate strain
μ	Viscosity
μ	Ductility
ν	Poisson's ratio
Ψ	Dilation angle (°)

List of Tables

List of Figures

Chapter 1 - Introduction

1.1 General

Central Asia countries are located in the region where Indo-Australian and Eurasian lithospheric plates collide (Wieland et al., 2014). The latest large earthquake that happened in Kazakhstan territory was the Chon-Kemin earthquake in 1911, which destroyed most of Almaty city. Its magnitude was Ms 8.0, and the fault, the source causing the earthquake, was 50 km away, in Kyrgyzstan. Thus, Almaty, a city along the Tien Shan Mountain range front, is vulnerable to earthquake activities (Overseas Development Institute, 2016). More than 50 % of the buildings in Almaty city are unreinforced masonry structures, then reinforced masonry, wooden and steel structures (Amey et al., 2021)

Unreinforced masonry is the oldest and most commonly used material type in building construction worldwide, and Kazakhstan is no exception. It is popular for its poor performance under lateral seismic force. Moreover, buildings of post-Soviet Union countries' seismic response capacity is much lower than officially stated (Wieland et al., 2014). Unreinforced masonry walls are one of the most vulnerable structures to seismic actions. The high vulnerability of the wall to seismic activities is related to the material properties of unreinforced masonry, low ductility, low tensile strength, and weight of the structure. Strengthening of unreinforced masonry walls is needed to improve the load-bearing capacity of the wall during earthquake activities. Researchers have studied extensive retrofitting techniques to enhance the behavior of unreinforced masonry buildings (Deng & Yang, 2018). Existing retrofitting techniques include strengthening the junctions of unreinforced masonry (URM) walls, textile-reinforced mortar, steel reinforced grout, and mortar joint treatment. The listed approaches are rarely used since these techniques significantly add weight to the structure. Surface treatment is the most widely used retrofitting technique which can improve the performance of existing URM structures under cyclic activities. Shortcreting and ferrocement are well-known as two types of surface treatment. Shortcreting can be attached to the steel wire mesh on one or both sides of the wall. However, it adds about 100 mm of concrete, which significantly increases the weight and may change the behavior of the whole structure. Ferrocement is also frequently treated to the surface of URM structures; however, steel reinforcement can corrode over time. This technique needs skilled labor forces, which is time-consuming, and may be costly. Moreover, ferrocement possesses limited fire resistance (Karantoni

& Fardis, 1992). Thus, additional retrofitting of the existing structure without adding any significant weight, using compatible, durable material is required. Fiber-reinforced polymer retrofitting is found as the technique that does not modify the weight of the wall; however, it behaves as elastic until the failure point, and due to the bond issues, its response becomes brittle along with debonding failure (Shrive, 2006). Recently, a new material called engineered cementitious composite or ECC, a material from the fiber-reinforced polymers class, was introduced as a retrofitting technique to enhance unreinforced masonry structures. According to the main finding of the literature review, existing normal-strength ECC retrofitting techniques increase the strength of the masonry, but not the ductility. Moreover, studies about URM walls with ECC retrofitting technique under cyclic loading conditions did not study the variation of the behavior of walls covered with different compressive strength ECC. They mainly elaborated on the other parameters such as mortar compressive strength, vertical pressure, geometry, etc. Therefore, this study observes the behavior of the URM walls retrofitted with different compressive strengths of the ECC and concentrates on low-strength engineered cementitious composite (ECC) as retrofitting material, which matches the stiffness of the masonry wall, and results in better ductility. The high ductility will avoid the high risk of damage to the masonry wall. It is assumed that the low-strength ECC can help spread out the cracks in the masonry wall and result in a more uniform damage pattern.

Numerical simulations were performed using the finite element method to study the behaviors of the unreinforced masonry walls under cyclic seismic forces. The numerical simulation of the wall test is a time-efficient study rather than large-scale experimental wall tests. The wall is analyzed using simplified micro modeling via ABAQUS 6 software.

The proposed research will analyze the effect of low-strength engineered cementitious composite on the performance of URM walls under cyclic loading. Although, many experimental studies have shown that normal strength ECC can enhance the strength and stiffness of the URM walls (Deng & Yang, 2018), it has limited ductility and deformation capacity improvement of the wall. Thus, this thesis will focus on the impact of low-strength ECC retrofit on the masonry wall. This study is built upon a prior study by Sailauova (2022) about pushover analyses of the unreinforced masonry wall covered with engineered cementitious composite (ECC) under monotonic loading. Cyclic seismic loading scenarios were introduced in this thesis work to align with actual earthquake conditions. A verified model was utilized for the parametric study to

examine the effect of ECC compressive strength, wall aspect ratio, and vertical pressure on the wall. Based on a parametric study, it is expected to propose the optimal parameters of ECC resulting in higher deformation capacity, high ductility, and reasonable overstrength of the URM walls, which can withstand cyclic seismic loadings.

1.2 Research hypothesis

1. Analytical models can capture the cyclic behavior of masonry walls with and without ECC.

2. The ductility of the masonry wall under cyclic loadings can be improved with the low-strength ECC.

3. Due to cumulative damages, the response of unreinforced masonry walls under cyclic loadings may differ from that under monotonic loading.

1.3 Objectives

This thesis concentrates on the study of the effect of retrofitting low-strength ECC to the masonry wall. The objectives of the study were established to achieve this aim. The key objectives of this study are listed below:

1. Develop analytical models for cyclic analyses on masonry walls with and without ECC.

2. Investigate behaviors of masonry walls with and without ECC under in-plane cyclic loadings.

3. Evaluate the effects of ECC strength on the seismic performance of retrofitted masonry walls.

Chapter 2 - Background

2.1 In-plane failure modes of masonry walls

Masonry walls under different external loading conditions can have various failure modes. Scholars keep investigating the different key parameters affecting the performance of unreinforced masonry walls or their failure modes (Hu et al., 2023). Generally, the main factors affecting the failure modes are the overall wall aspect ratio, boundary conditions, and vertical load (Magenes & Calvi, 1997). Two major failure types of the wall known are shear and flexural failure, as drawn in Figure 2.1 (Türkmen et al., 2019).

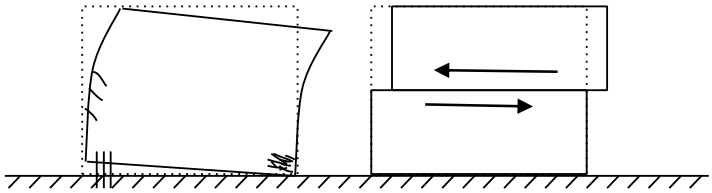

Figure 2.1. Flexural and shear failure representation.

Based on URM walls studies, walls with lower aspect ratios are more likely to experience shear failure, while the walls with higher aspect ratios achieve flexural failure. As for vertical pressure, with the increase of floor in masonry buildings, the vertical pressure will be increased roughly to 0.10 MPa (Hu et al., 2023). Figure 2.2 shows the in-plane failure modes of masonry walls namely diagonal shear failure, sliding failure, rocking, and toe crashing (Choi et al., 2023).

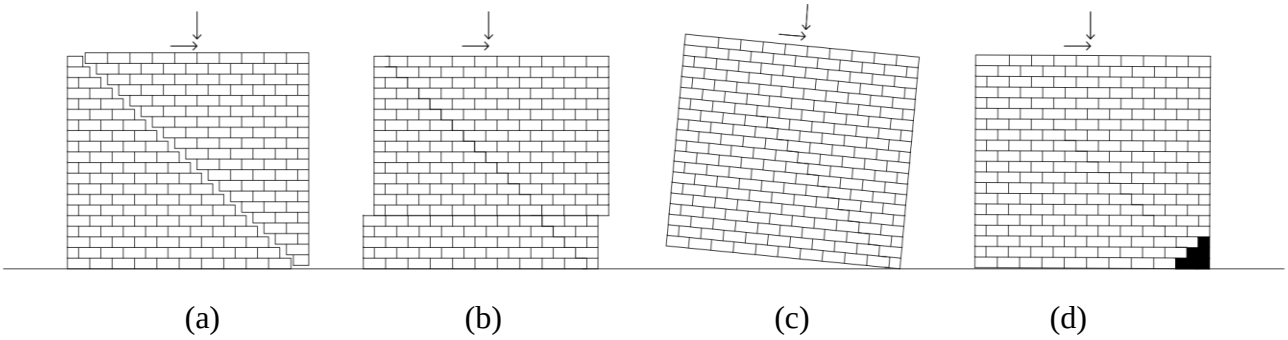

Figure 2.2. In-plane failure modes of masonry walls: (a) diagonal shear failure, (b) sliding failure, (c) rocking, (d) toe crashing based on ElGawady et al. (2006)

Diagonal shear failure happens along the mortar in stepped stair format. This is due to the separation of masonry unit and mortar, which is caused by the loss of bond between them. Sliding failure occurs along the specific bed joint, caused by the unit-mortar bond failure (Babaeidarabad et al., 2014). Rocking takes place at the bottom brick layer of the wall, accompanied by some uplift behavior of toe crushing (Choi et al., 2023). Wall experiences toe-crushing failure when the stress at the toe of the wall reaches the compressive strength of the masonry (Babaeidarabad et al., 2014). Choi et al. elaborate on experimental studies, where the walls with high deformation capacity and ductility failed at rocking and sliding behaviors. Most studies agree that rocking and sliding failures are ductile, less harmful failure modes, while diagonal shear failure and toe crushing are brittle and more harmful failure modes. The latter two undesired failure modes, because they are very brittle and happen suddenly. They may significantly damage the wall, and go across the bricks, while former two's damage happen gradually, and go through the mortar (Mustafaraj & Yardim, 2019).

2.2 Different retrofitting techniques for unreinforced masonry walls

URM structures are vulnerable to earthquakes, thus it is crucial to use strengthening techniques to elevate the load-carrying capacity of the structures. For that purpose, various retrofitting techniques eliminate the limitations of the design or construction process to become sufficiently seismic resistant. Two commonly used methods of retrofitting masonry walls are troweling and surface treatment.

Regardless of the plain direction of the target, surface treatment can be applied to strengthen the existing structure. There are 2 types of surface treatment: shotcrete and ferrocement techniques. The first type is spraying the shotcrete over the steel mesh of wire. The thickness of the coat, which ranges from 70 mm to 150 mm, is needed, and it varies according to seismic force (Pareek et al., 2016). Shear dowels are used to provide shear between shotcrete surfaces and masonry (ElGawady et al., 2006). The second type, ferrocement, includes multi-layers of mesh placed in 15-30 MPa high-strength cement mortar with 10-15 mm thickness (ElGawady et al., 2004). In cyclic tests, the ferrocement method improved the in-plane lateral resistance (Abrams et al., 2001). Kadam et al. (2014) explored that 0.29% of reinforcement in vertical strengthens URM in out-of-plane direction by 10 times.

Surface treatment approaches may significantly increase the weight of the structure and decrease the aesthetic of the structure. As for troweling, it minimizes concrete cracking, irregularities, and uneven drying. Except for hand trowels, nowadays troweling has various machines to complete the work, such as walk-behind, and ride-on trowels. However, they are intended to be used for large horizontal surfaces. A hand trowel can be used for the vertical surfaces of small-scale masonry walls (Hendry, 2001).

Therefore, recently troweling with various reinforcing composites has been introduced, such as additional externally attached composite overlays, fabric-reinforced cementitious matrix (FRCM), glass fiber reinforced polymer (GFRP), steel fiber reinforced concrete (SFRC) and fiber-reinforced polymer composites (FRP). FRP has advantages over the above-mentioned techniques, such as being lightweight, effective strengthening ability, and simple. However, it is not cost-effective and requires skills. Composites increase the lateral resistance by 1.1 to 3 times and out of plane stability (Alcaino et al., 2008).

2.3 A newly discovered retrofitting technique

Engineered cementitious composite (ECC) is one of the high-performance fiber-reinforced cementitious composites or HPFRCC based on the micromechanical properties of fiber-to-matrix bonds. ECC is a new retrofitting technique with high tensile ductility and multiple microcracks (Kyriakides et al., 2014). It has high tensile ductility due to tensile strain-hardening behavior with 3-5 % tensile strain, which is 300-500 times compared to normal fiber-reinforced concrete. Besides high tensile ductility, ECC features a 2% fiber volume fraction. ECC can keep crack width less than 100 micrometers. Due to its high tensile ductility and small crack width, ECC has high durability than normal concrete (Huang et al., 2013). Recently, ECC has been used in various applications, such as dam retrofitting and seismic resisting material for structures (Kyriakides et al., 2014). Overall, ECC showed significant improvement in behavior of the retrofitted structural elements (Niasar et al., 2020). ECC does not contain coarse aggregate since it impacts the ductile behavior of composite. Mixing components are cement, fine silica sand, fly ash, polymeric fibers, a high range of water reducer admixtures, and water (Singh et al., 2019). To specify, ECC consists of a Portland cement paste with the low volume ratio of polymeric fibers, such as ultrahigh molecular weight polyethylene (UHMWPE) or polyvinyl alcohol (PVA). These fibers give the ECC 2 to 8 MPa tensile strength (Niasar et al., 2020). ECC can incorporate the recycled industrial wastes, such as iron ore, fly ash and slag to decrease the cement content (Huang et al., 2013). The

effect of ECC on behavior of unreinforced masonry walls were tested in an experimental test by Deng and Yang (2018). In their study, three walls including one unretrofitted wall as reference wall, and two retrofitted walls by ECC in strip pattern and ECC cover with constant thickness. The results revealed that retrofitting techniques increased the lateral strength of the masonry wall. The unretrofitted wall resulted diagonal failure mode, while retrofitted walls showed rocking failures. Trowelling ECC to the whole wall helps avoid diagonal cracks in the wall and turns it into rocking mode. According to the Chapter 2.1 the rocking failure is more desired damage rather than diagonal failure mode. Failure modes of masonry walls described above are demonstrated in Figure 2.2. Deng and Yang (2018) concluded that parameters such as wall geometry, retrofitting method, and loading conditions can vary the lateral strength of the retrofitted wall, failure mode, and energy dissipation.

Wang and Li (2003) found that low-strength ECC has high tensile strain hardening, lightweight, low thermal conductivity, and acoustic insulation properties. URM walls retrofitted with ECC are expected to become seismic resistant. The lightweight filler technologies such as polymeric micro-hollow bubble, glass micro-hollow bubble, air-entrainment admixture and natural lightweight perlite were successfully applied in the development of lightweight ECC to retrofit URM walls (Wang & Li, 2003).

Zhu et al. (2018) studied the low-strength ECC for structural retrofit, and pushover analysis showed that low-strength ECC can increase strength and ductility of the masonry wall under in-plane and out-of-plane loading conditions. Moreover, the overall ductility was higher for the out-of-plane loading, because of flexural controlled deformation in out-of-plane direction.

2.4 Numerical modeling approach

Abdulla et al. (2017) examine the simulation response of the two-dimensional (2D) non-linear behavior of masonry walls under monotonic and cyclic in-plane, out-of-plane loading conditions. The study was conducted using finite element methods software ABAQUS. Based on the required accuracy and precision, numerical modeling has two major modeling approaches: micro and macro modeling (Doran et al., 2022). Micro-modeling is represented simplified micro-modeling and detailed micro-modeling. In detailed micro-modeling brick units and mortar are considered continuum elements and bed head joints of mortar represent unit-mortar interfaces as discontinuum elements. In this approach three components, brick unit, mortar, and unit-mortar interface, are modeled separately, acquiring proper constitutive law for each.

However, detailed micro-modeling (Figure 2.3a) is computationally intensive and can be limited by the number of elements. This may be used for more localized structures to find detailed and accurate results. The simplified modeling approach (Figure 2.3b) can be introduced to escape these limitations. In this approach, units expanded, including the mortar, and were considered continuum elements, while interactions were considered discontinuum elements. The simplified micro-modeling method is commonly used in numerical analyses due to its ease, low computational time, and cost compared to detailed micro-modeling. In the macro model (Figure 2.3c), the structure is considered as a homogeneous continuum material, without any separation between components. This approach can be used for complex structures to decrease the computational time and cost, but it cannot show detailed failure modes (Lourenço et al., 1994). Figure 2.3 summarizes the demonstrative difference between the detailed micro-modeling approach, simplified micro-modeling, and macro-modeling approaches.

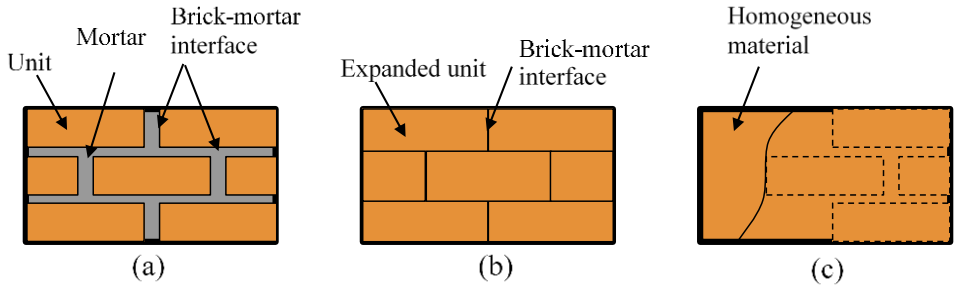

Figure 2.3. Finite element modeling approaches: (a) detailed micro-model; (b) simplified micro-model; (c) macro-model based on Abdulla et al. (2017)

Considering the advantages of simplified micro-modeling over other approaches, this method is most suitable for the numerical analysis of 2D unreinforced masonry walls with 20 layers of bricks under cyclic loading. It will allow us to study each component and global behavior of the wall with low computational time.

Chapter 3 - Parametric Study

3.1 Prototype Structure

According to KAZNIISA, Final Report II, and Main Report I, masonry buildings are defined as residential building series 308 (OYO International, 2009). To study the performance of masonry walls subjected to varied vertical pressure, the interior walls of 4 story masonry building series 308 were considered as prototype structure for the parametric study.

Since the aspect ratio is height divided by the width of the wall, for this study it was decided to keep the height of the wall constant, as it is for actual buildings' floor height, and vary the width of the wall. For the wall model for the numerical analysis, one-third scale of the real wall was used due to the large computational time needed to finish the simulation.

The aspect ratio of the prototype and model walls is given in Table 3.1.

Table 3.1. Prototype and model wall dimensions

Aspect ratio	**Prototype wall dimensions**		**Model wall dimensions**	
	Length (mm)	**Height (mm)**	**Length (mm)**	**Height (mm)**
0.50	6000	3000	2400	1250
0.75	4000	3000	1680	1250
1.00	2800	3000	1320	1250

Based on this document, the vertical pressure of traditional residential masonry buildings is calculated. Since most post-Soviet Union buildings have three to five floors, this study concentrates on the 3, 4, and 5 story buildings. Thus the corresponding vertical pressures are calculated in Table 3.2. The vertical load capacities of the walls of 3, 4, and 5 story prototype buildings were considered, and vertical pressures 0.43, 0.60, and 0.78 MPa or axial force ratio 0.10, 0.15 and 0.19 were used for the parametric study.

Table 3.2. Vertical pressure calculation

Number of floors	**3**	**4**	**5**
Typical floor dead load (kPa)	7.35		
Roof dead load (kPa)	4.39		
Live load (kPa)	2.00		
Axial load for the prototype wall (kN)	742.91	1037.80	1341.51
Axial load for the model wall (kN)	247.64	345.93	447.17
Cross-section area of the model wall (mm^2)	576 000		
Vertical pressure (Mpa)	0.43	0.60	0.78

3.2 Study parameters

This study will investigate three parameters: the aspect ratio of the masonry wall, the vertical pressure experienced by the wall, and the compressive strength of ECC. Table 3.3 summarizes the planned parameter values and Table 3.5 shows the detailed input parameters for the parametric study. Aspect ratios 0.5, 0.75, and 1.0 were chosen based on a prototype building in Almaty, Kazakhstan. The vertical load capacity of the walls for the different-story prototype building was calculated as 0.43, 0.60, and 0.78 MPa. A detailed description of the aspect ratio and vertical pressure can be found in Chapter 3.1. As mentioned in the above chapters, ECC strength is that fc 10, 20, and 30 MPa are considered low-strength ECC, whereas fc 40, 50 MPa as normal-strength ECC. Wang and Li (2003) in their paper, order to achieve the low-strength ECC used hollow glass bubbles, polymeric microform, and perlite known as lightweight fillers or aggregate mixed with the air entrainment admixture. Hollow glass bubble filler acted as the agent to lower the density of the ECC.

Table 3.3. Summary table of study parameter values.

Aspect ratio			Vertical pressure (MPa)			Compressive strength of ECC (MPa)				
0.5	0.75	1.0	0.43	0.60	0.78	10	20	30	40	50

For the different strengths of ECC, the various experimental data from many researchers were studied. All data from the test were used to find the trendline for the ECC compressive strength versus density, elastic modulus, cracking strength, and peak tensile strength graphs. Based on the trendline equation, the variation of those parameters was calculated for the ECC compressive strength 10, 20, 30, 40, and 50 MPa. Except for the ECC compressive strength depending on variables, some parameters had fewer changes. Thus, these values were considered fixed parameters. Fixed parameters can be found in Table 3.4.

Table 3.4. Summary table of fixed parameters for ECC based on Sailauova (2022).

Compressive strain at peak stress, ε_0	Compressive residual strain, ε_r	Compressive ultimate strain, ε_u	Tensile strain at peak stress, ε_{tp}	ensile ultimate strain, ε_t
0.0045	0.0075	0.02	0.03	0.033

Run matrix with varying parameters can be found in Table 3.5. The total number of runs with monotonic runs is 90 and the masonry wall without ECC runs are 18. For the parametric study, it was necessary to complete 108 runs in total.

Table 3.5. Summary table of varying parameters of the study based on Sailauova (2022).

Run #	AR	ECC-fc (MPa)		Number of stories	Vertical P (MPa)	Loading type	Density (kg/m^3)	ECC-Young's Modulus (Gpa)	ECC Compressive behavior			ECC Tensile behavior		
									σ0 (MPa)	σr (MPa)	σu (MPa)	σt0 (MPa)	εt0	σtp (MPa)
1	0.5	Low-strength	10	3-story	0.43	Cyclic/Mon	903	2.87	10	4	1.5	1.37	4.78E-04	2.03
2			20	3-story	0.43	Cyclic/Mon	1128	6.28	20	8	3	1.93	3.08E-04	2.72
3			30	3-story	0.43	Cyclic/Mon	1354	9.69	30	12	4.5	2.50	2.58E-04	3.40
4		Normal-strength	40	3-story	0.43	Cyclic/Mon	1580	13.10	40	16	6	3.07	2.34E-04	4.09
5			50	3-story	0.43	Cyclic/Mon	1806	16.51	50	20	7.5	3.63	2.20E-04	4.78
6	0.5	Low-strength	10	4-story	0.6	Cyclic/Mon	903	2.87	10	4	1.5	1.37	4.78E-04	2.03
7			20	4-story	0.6	Cyclic/Mon	1128	6.28	20	8	3	1.93	3.08E-04	2.72
8			30	4-story	0.6	Cyclic/Mon	1354	9.69	30	12	4.5	2.50	2.58E-04	3.40
9		Normal-strength	40	4-story	0.6	Cyclic/Mon	1580	13.10	40	16	6	3.07	2.34E-04	4.09
10			50	4-story	0.6	Cyclic/Mon	1806	16.51	50	20	7.5	3.63	2.20E-04	4.78
11	0.5	Low-strength	10	5-story	0.78	Cyclic/Mon	903	2.87	10	4	1.5	1.37	4.78E-04	2.03
12			20	5-story	0.78	Cyclic/Mon	1128	6.28	20	8	3	1.93	3.08E-04	2.72
13			30	5-story	0.78	Cyclic/Mon	1354	9.69	30	12	4.5	2.50	2.58E-04	3.40
14		Normal-strength	40	5-story	0.78	Cyclic/Mon	1580	13.10	40	16	6	3.07	2.34E-04	4.09
15			50	5-story	0.78	Cyclic/Mon	1806	16.51	50	20	7.5	3.63	2.20E-04	4.78
16	0.8	Low-strength	10	3-story	0.43	Cyclic/Mon	903	2.87	10	4	1.5	1.37	4.78E-04	2.03
17			20	3-story	0.43	Cyclic/Mon	1128	6.28	20	8	3	1.93	3.08E-04	2.72
18			30	3-story	0.43	Cyclic/Mon	1354	9.69	30	12	4.5	2.50	2.58E-04	3.40
19		Normal-strength	40	3-story	0.43	Cyclic/Mon	1580	13.10	40	16	6	3.07	2.34E-04	4.09
20			50	3-story	0.43	Cyclic/Mon	1806	16.51	50	20	7.5	3.63	2.20E-04	4.78
21	0.8	Low-strength	10	4-story	0.6	Cyclic/Mon	903	2.87	10	4	1.5	1.37	4.78E-04	2.03
22			20	4-story	0.6	Cyclic/Mon	1128	6.28	20	8	3	1.93	3.08E-04	2.72
23			30	4-story	0.6	Cyclic/Mon	1354	9.69	30	12	4.5	2.50	2.58E-04	3.40
24		Normal-strength	40	4-story	0.6	Cyclic/Mon	1580	13.10	40	16	6	3.07	2.34E-04	4.09
25			50	4-story	0.6	Cyclic/Mon	1806	16.51	50	20	7.5	3.63	2.20E-04	4.78
26	0.8	Low-strength	10	5-story	0.78	Cyclic/Mon	903	2.87	10	4	1.5	1.37	4.78E-04	2.03
27			20	5-story	0.78	Cyclic/Mon	1128	6.28	20	8	3	1.93	3.08E-04	2.72
28			30	5-story	0.78	Cyclic/Mon	1354	9.69	30	12	4.5	2.50	2.58E-04	3.40
29		Normal-strength	40	5-story	0.78	Cyclic/Mon	1580	13.10	40	16	6	3.07	2.34E-04	4.09
30			50	5-story	0.78	Cyclic/Mon	1806	16.51	50	20	7.5	3.63	2.20E-04	4.78
31	1	Low-strength	10	3-story	0.43	Cyclic/Mon	903	2.87	10	4	1.5	1.37	4.78E-04	2.03
32			20	3-story	0.43	Cyclic/Mon	1128	6.28	20	8	3	1.93	3.08E-04	2.72
33			30	3-story	0.43	Cyclic/Mon	1354	9.69	30	12	4.5	2.50	2.58E-04	3.40
34		Normal-strength	40	3-story	0.43	Cyclic/Mon	1580	13.10	40	16	6	3.07	2.34E-04	4.09
35			50	3-story	0.43	Cyclic/Mon	1806	16.51	50	20	7.5	3.63	2.20E-04	4.78
36	1	Low-strength	10	4-story	0.6	Cyclic/Mon	903	2.87	10	4	1.5	1.37	4.78E-04	2.03
37			20	4-story	0.6	Cyclic/Mon	1128	6.28	20	8	3	1.93	3.08E-04	2.72
38			30	4-story	0.6	Cyclic/Mon	1354	9.69	30	12	4.5	2.50	2.58E-04	3.40
39		Normal-strength	40	4-story	0.6	Cyclic/Mon	1580	13.10	40	16	6	3.07	2.34E-04	4.09
40			50	4-story	0.6	Cyclic/Mon	1806	16.51	50	20	7.5	3.63	2.20E-04	4.78
41	1	Low-strength	10	5-story	0.78	Cyclic/Mon	903	2.87	10	4	1.5	1.37	4.78E-04	2.03
42			20	5-story	0.78	Cyclic/Mon	1128	6.28	20	8	3	1.93	3.08E-04	2.72
43			30	5-story	0.78	Cyclic/Mon	1354	9.69	30	12	4.5	2.50	2.58E-04	3.40
44		Normal-strength	40	5-story	0.78	Cyclic/Mon	1580	13.10	40	16	6	3.07	2.34E-04	4.09
45			50	5-story	0.78	Cyclic/Mon	1806	16.51	50	20	7.5	3.63	2.20E-04	4.78

3.3 Analytical model

3.3.1 Geometry and element types

3.3.1.1 2D masonry wall model

In this thesis, the numerical simulation software based on finite element methods (FEM) called ABAQUS will be utilized to assess the responses of unreinforced masonry walls to cyclic seismic force (ABAQUS, 2010). The two-dimensional (2D) numerical model of the masonry wall will be built using a simplified micro-modeling method (Figure 2.3b). A summary of numerical modeling approaches can be found in Chapter 2 - Background. In the simplified micro-modeling method, mortar and brick units are merged, so the brick unit is considered expanded. Two main analytical wall models with 20 levels of masonry units and single wythe brick were built. One is the masonry wall without the ECC model, and the other is with ECC retrofit attached to the masonry wall model.

3.3.1.1.1. 2D masonry wall model without ECC

Figure 3.1 shows the numerical model of the unreinforced masonry walls, where brick units are homogeneous solids, modeled with concrete damaged plasticity. Bricks are interacted through friction and spring cohesion. The model walls were subjected to lateral cyclic loading and uniformly distributed gravity load. Boundary conditions of both walls are pinned bottom nodes and the top, and bottom levels of the wall are considered as elastic material acting as the top beam and foundation of the wall, respectively.

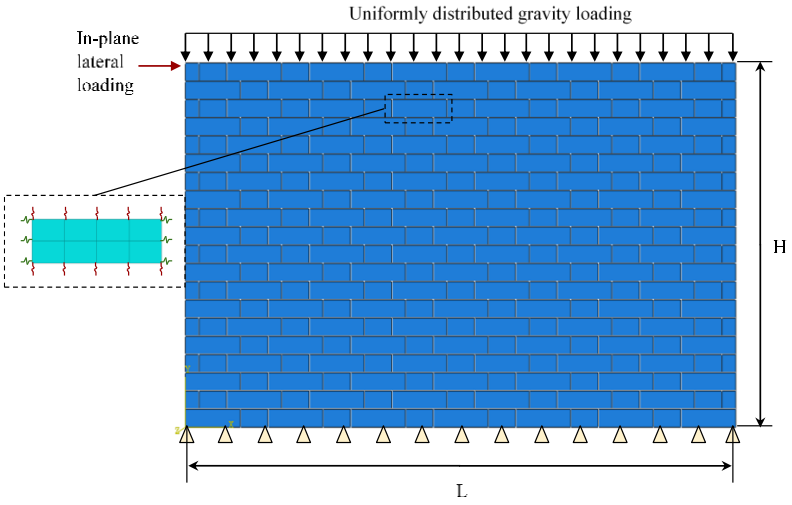

Figure 3.1. Analytical 2D masonry wall model without ECC.

3.3.1.1.2. 2D masonry wall model with ECC

The analytical 2D wall model retrofitted with ECC material is shown in Figure 3.2. The ECC retrofitted model has the same masonry wall properties. The ECC layer was attached to the wall by tie constraints. In order to avoid undesired deformation, the ECC is meshed so that nodes of its triangular elements are tied with the central internal nodes of the brick units.

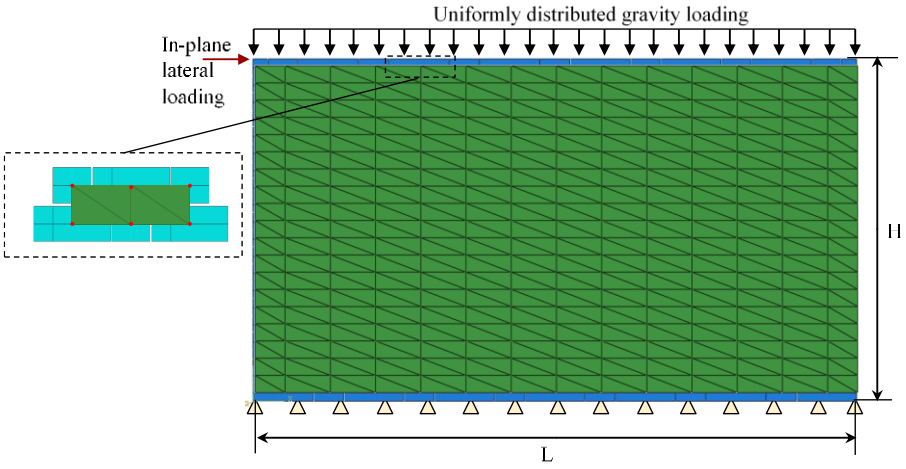

Figure 3.2. Analytical 2D masonry wall model with ECC.

3.3.2 Materials models

3.3.2.1 Masonry units

The nonlinear behavior of masonry units was simulated using the concrete damaged plasticity (CDP) model. The CDP model captures the isotropic damaged elasticity and isotropic compressive and tensile plasticity (ABAQUS, 2010). The plasticity parameters for the CDP model were chosen, as shown in Table 3.6, and determined as appropriate to meet the experimental results.

Table 3.6. CDP model for masonry

Dilation angle	Eccentricity	*fb0/fc0*	Kc	Viscosity	Poisson's ratio
30	0.1	1.16	0.667	0	0.15

The compressive crushing behavior of the masonry units is described in the uniaxial compressive stress-strain curve in Figure 3.3.

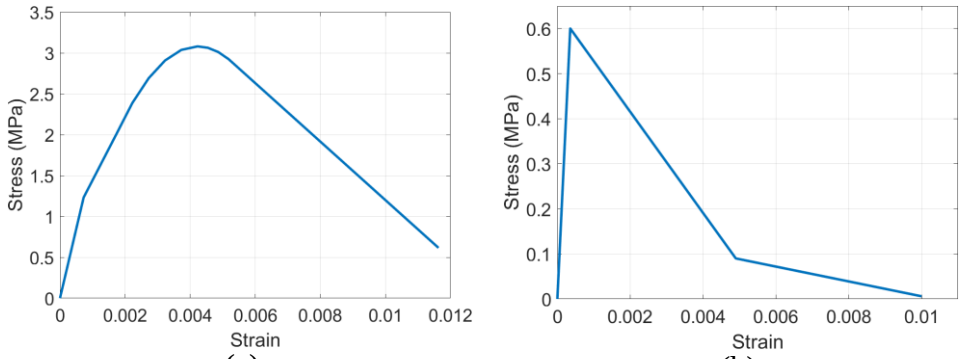

Figure 3.3. (a) Compression and (b) tension stress-strain curves of the CDP model for the masonry.

The tensile behavior depends on the localized cracks, after elastic performance before the peak, followed by the bi-linear softening behavior. In the numerical model, the inelastic part of the curves was introduced. The peak compressive strength was calculated according to the GB 50010-2010, Code for the design of masonry structures.

$$f_w = 0.78 f_b^{0.5}(1 + 0.07 f_m) \tag{3.1}$$

, where f_w , f_b , f_m are average compressive strength of wall, brick, and mortar, respectively. The elastic behavior of the model was adjusted since the numerical study was conducted using a simplified micro-modeling approach. Abdulla et al. 2017 proposed the equation to adjust the masonry elastic modulus by considering the elastic modulus of unit bricks and mortar, along with the geometry.

$$E_w = \frac{H E_b E_m}{n h_b E_m + (n-1) h_m E_b} \tag{3.2}$$

, where E_w , E_b , E_m are elastic modulus of the wall, brick, and mortar, respectively. H , h_b , h_m are the height of the masonry wall, the height of the brick unit, and mortar thickness respectively. n is the number of brick levels. Based on the mechanical properties of brick and mortar, the adjusted masonry wall properties were calculated as in Table 3.7.

Table 3.7. Material properties of masonry.

Elastic modulus, MPa	**Compressive strength, MPa**	**Tensile strength, MPa**
1694	3.08	0.60

3.3.2.2 Mortar

In the numerical model, in order to give mortar properties, the combination of connectors and friction interactions was used. The cohesion or connectors were designed as bed and head spring joints. Bed joints were used to connect vertically, while head joints were for horizontal connections. Two types of joints were designed depending on the corresponding tributary areas of the masonry. There are external and internal head and bed joints. Friction was applied using surface-to-surface contact of two possible surfaces that directly contact each other, with a friction coefficient of 0.75. The material properties of the mortar joints were calculated based on Abdulla's paper (2017). Table 3.8 summarizes the properties as follows:

Table 3.8. Mortar joints properties

Tangential behaviour			Normal behaviour	Cohesive behaviour		Damage				
Friction coefficient	Shear stress limit, MPa	Max. elastic slip (as a fraction of surface dimension)	Hard contact	K_{nn}, N/mm^3	K_{ss}, N/mm^3	t_n^{max}, MPa	t_s^{max}, MPa	G_{IC}, N/mm	G_{IIC}, N/mm	Viscosity coefficient
0.75	4.325	0.005	-	47.1	20.5	0.201	0.575	0.022	0.22	0.002

3.3.2.3 ECC

The CDP model was also used to simulate the non-linear behavior of the ECC, with the combination of the brittle cracking model. The plasticity parameters for the ECC CDP model were similar to those of the masonry, except for viscosity, which for ECC is 0.001.

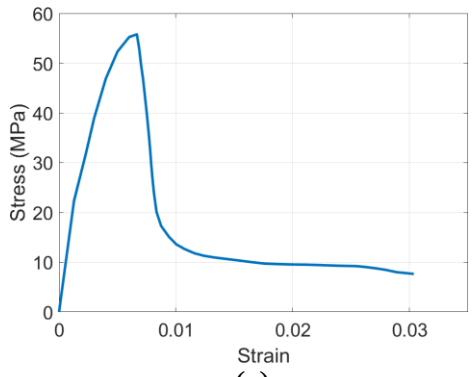

(a)

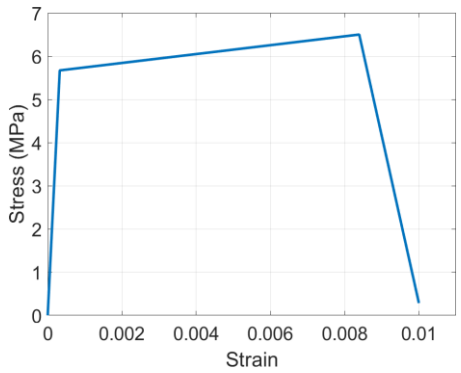

(b)

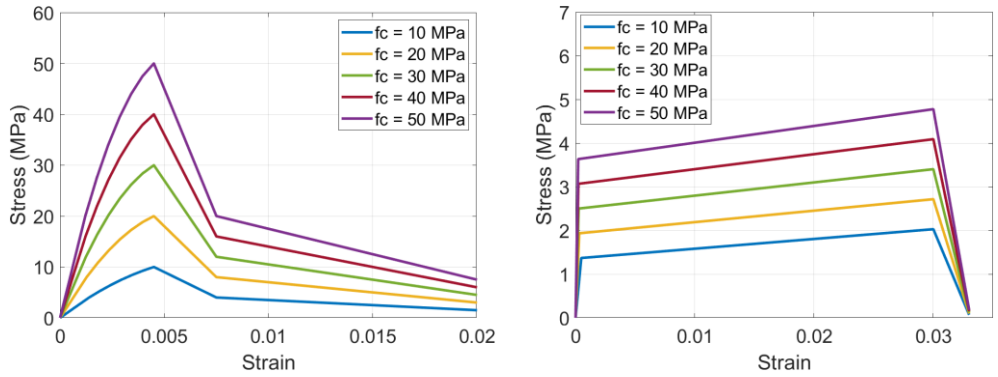

Figure 3.4. (a) Compression and (b) tension stress-strain curves of the CDP model for the ECC used for model calibration, (c) compression and (d) tension stress-strain curves of the CDP model for the ECC used for parametric study.

Figure 3.4 depicts the nonlinear behavior of the ECC. The compression stress-strain curve is elastic until 40 % of the peak compressive strength, and the post-peak phase follows the drop to the residual stress, which is also 40 % of the peak stress. Then gradually, it reaches the ultimate stress, which is 15% of the peak stress. The tension stress-strain curve indicates cracking strength, gradually rises with the tensile strain to the peak strength, and drops ultimate strength, 5% of the cracking stress.

The combination of the brittle cracking model was crucial since the single CDP model for the ECC exhibited dominating brittle behavior under the cyclic loading. Thus, the brittle cracking model assisted in assuming that ECC is linearly elastic in compression. The same tensile behavior as in the CDP model was used for the brittle cracking. The brittle shear option was introduced. Brittle cracking parameters applied are shown in Tables 3.9-3.10.

Table 3.9. Brittle cracking model for ECC

f_t	0.6	0.09	0.006
Cracking strain	0.00000	0.00486	0.01000

Table 3.10. Brittle Shear

Shear retention factor	1.0	0.3	0.01	0
Cracking opening strain	0	0.001	0.002	0.01

3.3.3 Loading condition

This study examines the effect of ECC under different composite compressive strengths, wall geometries, and subjected vertical pressures. By varying the key parameters, such as wall aspect ratio, which is the ratio between wall width and height, and applied vertical pressure which imitates the pressure experienced in the 3,4 and 5 story prototype buildings from Almaty and compressive strength of wall retrofit. The loading protocol for the wall under cyclic loading is shown in Figure 3.5. It will start from 1 mm until 24 mm both loading and unloading with the loading rate set to 2 mm/s until the end of the simulation.

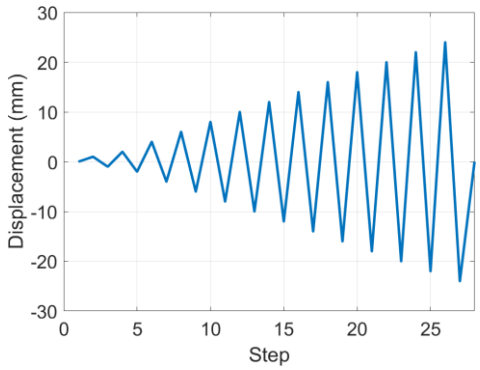

Figure 3.5. Loading protocol.

3.3.4 Model validation

The experimental wall test of masonry wall with and without ECC coating by Deng and Yang (2018) was used for model verification. Their study used 240 mm x 115 mm x 53 mm brick and 10 mm mortar. Two wythe masonry wall with 20 levels of masonry units and with dimensions of 2300 mm x 240 mm x 1250 mm. The bottom of the wall was fixed with a reinforced concrete beam, and an RC cap was placed at the top of the beam to spread the lateral load evenly. The specimen was subjected to a constant 0.5 MPa vertical pressure. In the test, wall loading was force-controlled until it cracked, and changed to displacement-controlled loading. The loading-unloading rate was 2 mm per cycle up to 8 mm displacement.

The wall geometry was modified according to a simplified micro-modeling approach for the model validation. For the 20 levels of masonry units with an overall 1250 mm height, the expanded unit was taken as 62.5 mm as merging brick unit and mortar thickness. In the analytical model instead of two wythe wall, the thickness of the wall is simplified to a single wythe 240 mm, and the length of the brick is 240 mm. Odd levels were modeled to have 7 full, and 6 half units,

while even levels have 6 full, 7 half, and 2 quarter units. Half unit is half the length of the full unit, and quarter unit is the quarter length of the full unit. Instead of the top and bottom concrete beams from the experiment, in numerical simulation, lateral loading to the top one-and-a-half level of masonry was applied, and fixed boundary condition at the bottom nodes were used. In the ECC retrofitted wall, for the two edges where the quarter units are, the ECC elements are 120 mm in length and the same 62.5 mm in height as the brick units. However, ECC elements connected with the half and full units are 180 mm in length, and the same in height.

The global responses to the model verification are illustrated in Figure 3.6.

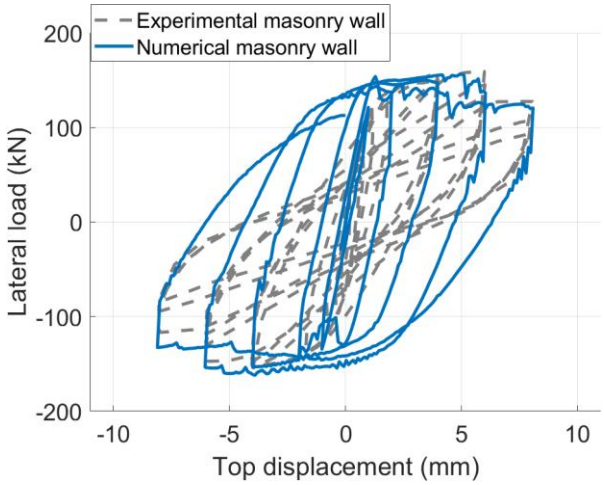

(a) Masonry wall only

Figure 3.6. Global response of the numerical simulation of bare wall compared to the test.

The wall only model showed quite similar behavior to that of the experimental test. A concrete damaged plasticity (CDP) model was introduced to ECC material in the monotonic loading study of Sailauova (2022) and showed a similar overall trend to the experimental results.

Thus, this study also checked for CDP for ECC material under cyclic loading. However, a quick strength drop was observed during model calibration, as shown in Figure 3.7a.

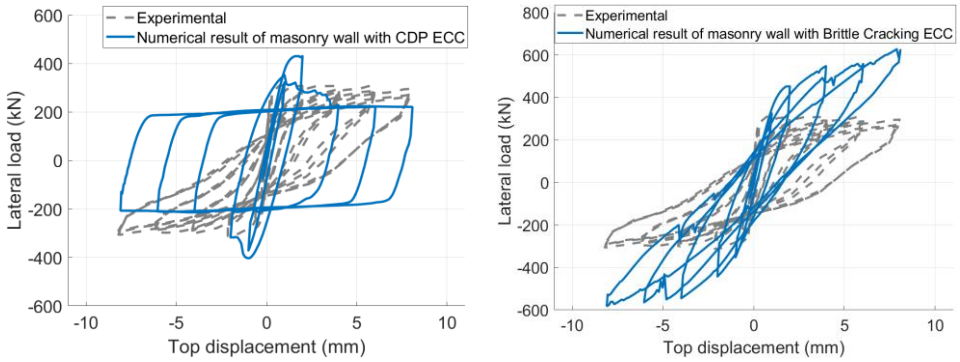

(a) (b)

Figure 3.7. Retrofitted walls designed with ECC (a) CDP and (b) Brittle Cracking models.

Therefore, the brittle cracking model was introduced to the ECC, which individually showed continuous strength rise as in Figure 3.7b. Brittle cracking is the most accurate model to apply for predominant brittle behavior, allowing the assumption of linear elastic behavior in compression to be sufficient. Brittle shear was used with the Brittle Cracking option.

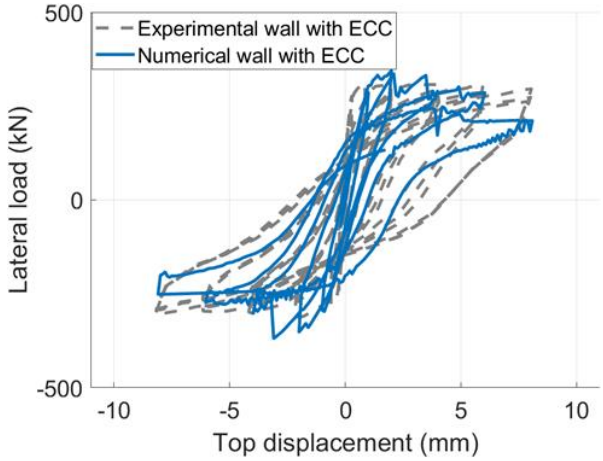

Figure 3.8. Retrofitted walls designed with ECC combined CDP and Brittle Cracking models.

The masonry wall with the ECC model shown in Figure 3.8 represents the case modeled with the combination of CDP and Brittle cracking models, which is the best matching model. This model experienced a smaller strength drop and no continuous strength increase. The deformation capacity of the ECC retrofitted wall model slightly differs from the experimental result. Overall, the curve trends are close to the test results. Thus, analytical models were utilized in a parametric study.

Chapter 4. Results

This chapter will provide the numerical results of cyclic analyses of the wall and parametric study. The parameters of the study are wall aspect ratio, vertical pressure, and ECC compressive strengths. The global behavior of the walls, deformation capacity, contours, component results, stiffness degradation, and energy dissipation results are demonstrated and discussed in this part of the thesis.

4.1 Global behavior of the masonry walls.

Global response for the masonry walls aspect ratio 0.5, 0.75, and 1.0 under 0.43 MPa, 0.60 MPa, and 0.78 MPa vertical pressures, as-built and retrofitted masonry wall with the 10 MPa, 20 MPa, 30 MPa, 40 MPa and 50 MPa compressive strength ECC retrofits will be presented in this section. These global behavior curves will assist in evaluating and observing the trends of the strength increase or degradation, displacement capacity of the masonry walls, and ductility of the walls. Furthermore, the global response will help summarize the results of different component contributions since the addition of cohesion and friction, if retrofitted wall ECC contribution equals the total global response of the masonry wall. The study parameters were applied to the numerical model, and hysteretic curves were obtained as in Figures 4.1-4.9.

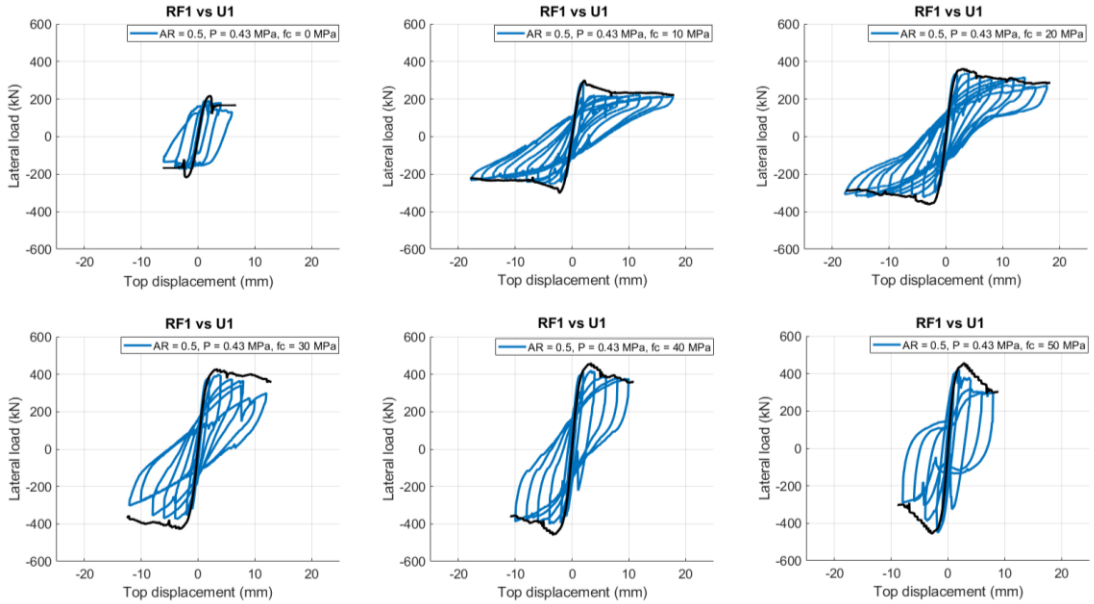

Figure 4.1. Global response of ECC retrofitted masonry wall with ECC compressive strength 0, 10, 20, 30, 40, 50 MPa under 0.43 MPa vertical pressure for aspect ratio 0.5.

Figure 4.1 illustrates the unretrofitted masonry (reference wall) and ECC retrofitted wall with ECC compressive strength (fc) 10, 20, 30, 40, and 50 MPa for wall aspect ratio 0.5, under 0.43 MPa vertical pressure. It is obvious that the unretrofitted masonry wall has smaller strength and less deformation capacity compared to the ECC-covered masonry walls. Compressive strengths 10, 20, 30, 40, and 50 MPa were studied to study the ECC strength effect. It can be observed that the strength of the ECC proportionally influences the overall wall strength. However, the deformation capacities of the walls are becoming less as the ECC becomes stronger, as has been hypothesized. The unretrofitted wall could resist up to 6 mm displacement, while masonry walls having ECC layer with strengths 10, 20, 30, 40, and 50 MPa could withstand up to 18, 18, 12, 10, and 8 mm displacements, respectively. The low-strength ECCs with 10 and 20 MPa induced smoother wall behavior, whereas from ECC 30 to 50 MPa the strength drop behavior of the wall was observed. The peak strength of the wall under cyclic load was considered the minimum absolute value of the loading and unloading stages. The unretrofitted wall reached 174 kN, while the retrofitted wall with ECC compressive strength 10, 20, 30, 40, and 50 MPa could handle 251, 332, 372, 399, and 419 kN, respectively. Adding the ECC to the URM wall, the low ECC compressive strength of 10 and 20 MPa increased the strength of URM wall to approximately 44 and 90%. The pushover curves are also shown in Figure 4.1 with a black line, resulting in lower cyclic loading than monotonic loading. The contrasting behavior between pushover and cyclic analysis was observed for the masonry wall with 30 MPa compressive strength ECC retrofit. The pushover curve resulted in a smoother curve, while the cyclic shows a strength drop at 12 mm displacement.

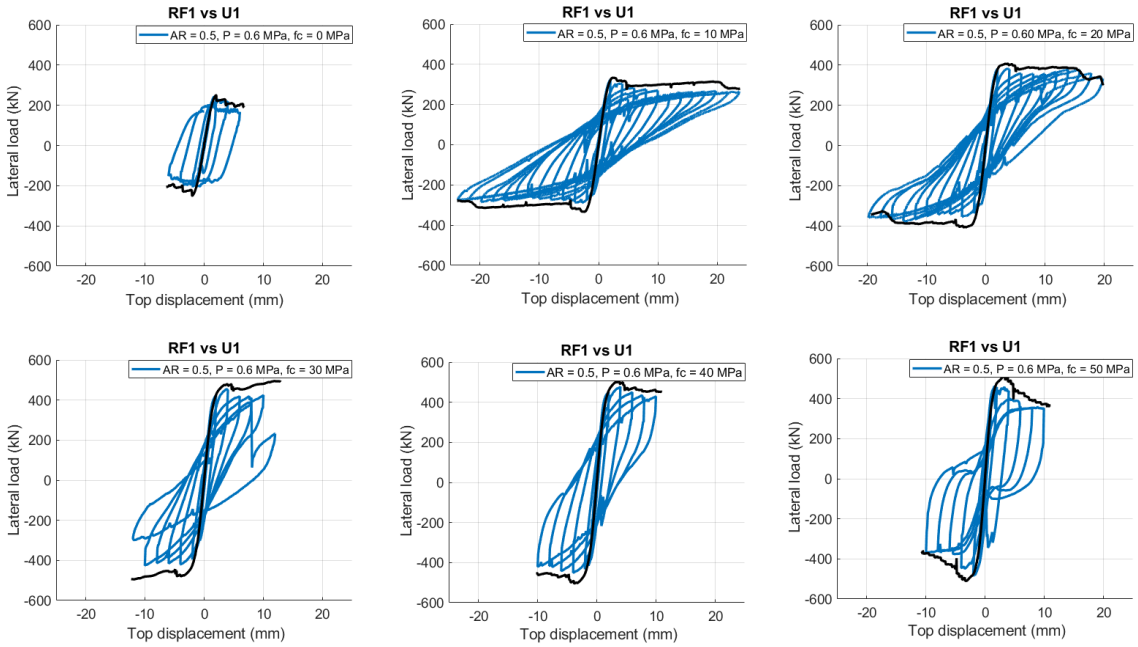

Figure 4.2. Global response of ECC retrofitted masonry wall with ECC compressive strength 0, 10, 20, 30, 40, 50 MPa under 0.60 MPa vertical pressure for aspect ratio 0.5.

Figure 4.2 shows the global results of masonry walls under 0.60 MPa vertical pressure. The global behavior of all remaining behaviors resulted in the same overall trend. As the vertical pressure rises to 0.60 MPa, the maximum strength of the walls becomes stronger than the vertical pressure of 0.43 MPa. Bare wall under 0.60 MPa axial pressure reached 207 MPa, whereas the retrofitted wall with ECC compressive strength 10, 20, 30, 40, and 50 MPa had 289, 359, 419, 451, and 460 kN peak strengths, respectively. Retrofitting composite added to the URM wall, the lowest ECC compressive strength of 10 MPa, was roughly 40% higher than URM wall strength. Applying the ECC layer to the bare wall with a deformation capacity of 6 mm, at least adds an additional 4 mm displacement, as in the case of 50 MPa ECC retrofit, but at most it can go up to 24 mm displacement with the 10 MPa ECC retrofit. In addition, the 20 MPa retrofit could withstand 20 mm displacement, while 30, 40, and 50 MPa demonstrated 12, 10, and 10 mm displacements respectively. This case also shows the descending displacement capacity with the ascending value of ECC layer compressive strength. Besides deformation capacity, the noticeable sharp strength drop can be observed between 40 MPa and 50 MPa reaching the same 10 mm displacements. Moreover, the black line pushover curves are higher than the backbones of hysteresis curves with the difference in strength.

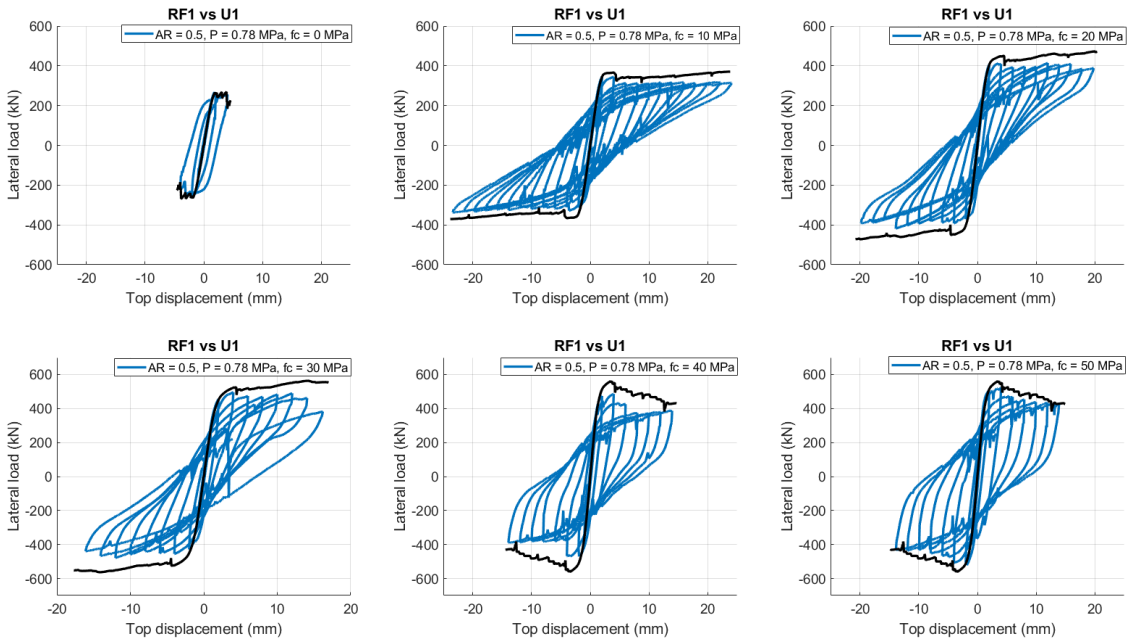

Figure 4.3. Global response of ECC retrofitted masonry wall with ECC compressive strength 0, 10, 20, 30, 40, 50 MPa under 0.78 MPa vertical pressure for aspect ratio 0.5.

Walls under high vertical pressure, 0.78 MPa, are presented in Figure 4.3. Vertical pressure of 0.78 MPa covered more wall strength rather than 0.60 and 0.43 MPa. Under this pressure, the URM wall achieved 246 MPa, whereas the retrofitted wall with ECC compressive strength 10, 20, 30, 40, and 50 MPa had 332, 392, 455, 471, and 521 kN peak strengths, respectively. At least, the low-strength ECC 10 MPa, increased bare URM wall strength to about 35%.

Walls with an aspect ratio of 0.5 under different vertical pressure conditions show how the strength of the masonry wall is gained with the increase of vertical pressure in Figures 4.1-4.3. Moreover, walls with ECC retrofit increase in strength and stiffness with the increase of compressive strength of retrofitting composite. The strength drop for the ECC compressive strengths 30 to 50 MPa can be observed. The deformation capacity of the walls decreases as the ECC becomes stronger and can confirm that this is applicable for other cases. As for the pushover curves, compared to the backbone curves of the hysteretic curves, there are strength differences at different stages of loading.

Figures 4.4-4.6 illustrates the ECC retrofitted wall with wall aspect ratio 0.75 for ECC compressive strength (fc) 10, 20, 30, 50 MPa, under 0.43, 0.60, 0.78 MPa vertical pressures.

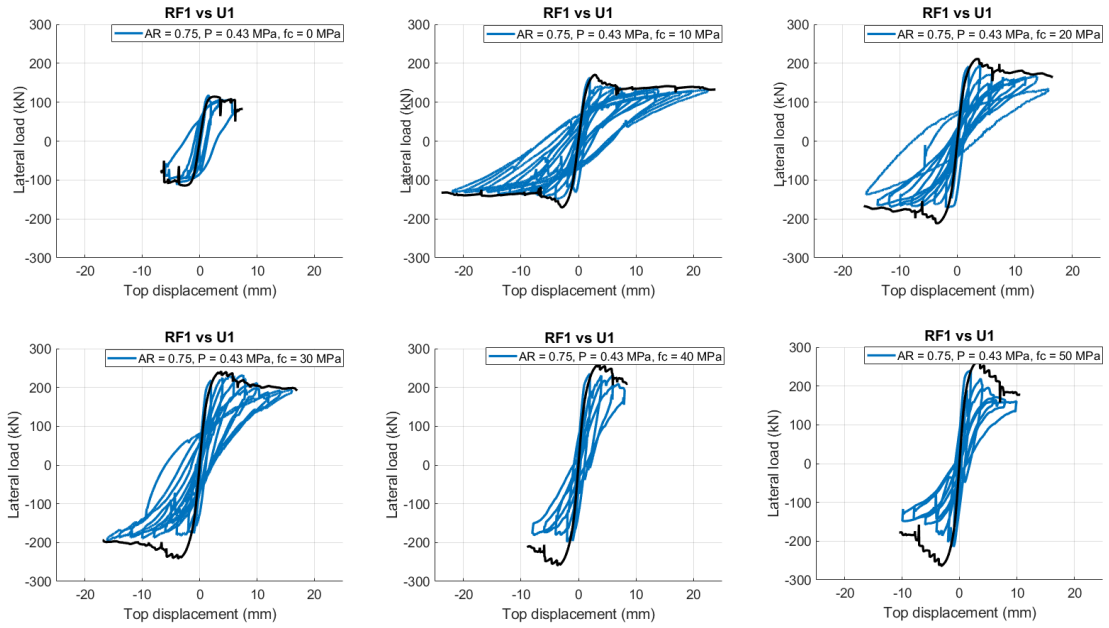

Figure 4.4. Global response of ECC retrofitted masonry wall with ECC compressive strength 0, 10, 20, 30, 40, 50 MPa under 0.43 MPa vertical pressure for aspect ratio 0.75.

Figure 4.4 illustrates the global results of the masonry walls with the aspect ratio 0.75 under vertical pressure 0.43 MPa, with different ECC compressive strengths. The ultimate displacement for the normal strength ECC is observed at the very early loading stage. The URM wall had 112 kN lateral strength, while ECC-covered masonry walls had the strength of 152, 171, 187, 198, and 215 kN for the ECC strength 10, 20, 30, 40, and 50 MPa, respectively. The strength rise for the fc 10 from the bare wall was 36%. The ECC strengths 40, and 50 MPa had narrow loops compared to the remaining strengths. Moreover, with the larger aspect ratio, the strength of the wall is reduced. For instance, a bare wall with an aspect ratio of 0.5 under 0.43 MPa had 174 kN, while a 0.75 aspect ratio resulted in 112 kN. The same pattern was observed for the ECC retrofitted walls and their pushover curves, which were preserved as in previous cases.

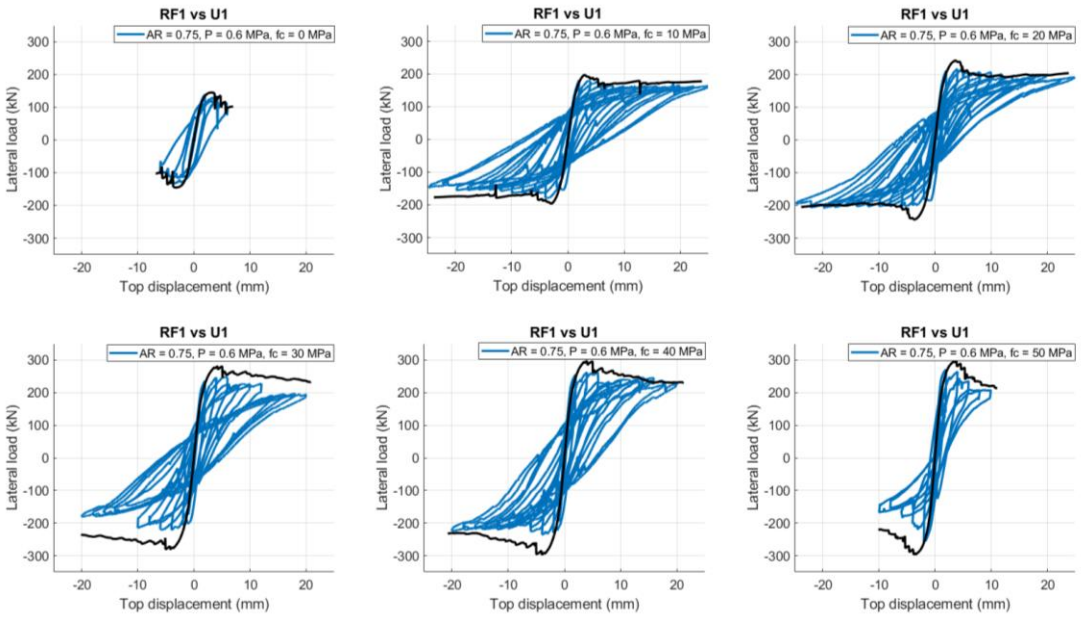

Figure 4.5. Global response of ECC retrofitted masonry wall with ECC compressive strength 0, 10, 20, 30, 40, 50 MPa under 0.60 MPa vertical pressure for aspect ratio 0.75.

Figure 4.5 shows the global behavior curves of the different ECC strength covered masonry walls with an aspect ratio of 0.75 under 0.60 MPa vertical pressure, including the masonry wall only. The masonry wall only obtained the 132 kN, 10, 20, 30, 40, and 50 MPa ECC retrofitted walls attained the 180, 197, 221, 236 and 258 kN wall strength. Retrofitting the wall with ECC strengthens the wall by at least 36%. Moreover, the higher ECC compressive strength retrofits resulted in early failure points, rather than low-strength ECCs, 10 MPa and 20 MPa. The low-strength ECC layers, improved the deformation capacity of the retrofitted wall from 6 mm displacement capacity to 25 mm displacement capacity, implying that adding the low-strength ECC to the masonry wall improves the ductility of the wall, and inhibits the damage rate during earthquakes. The case for aspect ratio 0.5 under 0.60 MPa had higher strength, as 207, 289, 359, 419, 451, and 460 kN for ECC retrofit strength 0, 10, 20, 30, 40 and 50 MPa. This can lead to the conclusion that increasing the aspect ratio decreases the wall's strength. However, the masonry wall, with an aspect ratio of 0.75 under applied moderate vertical pressure, had relatively higher strength than the applied low vertical pressure. As in previous cases, a strength difference was noticed in monotonic and cyclic loading responses.

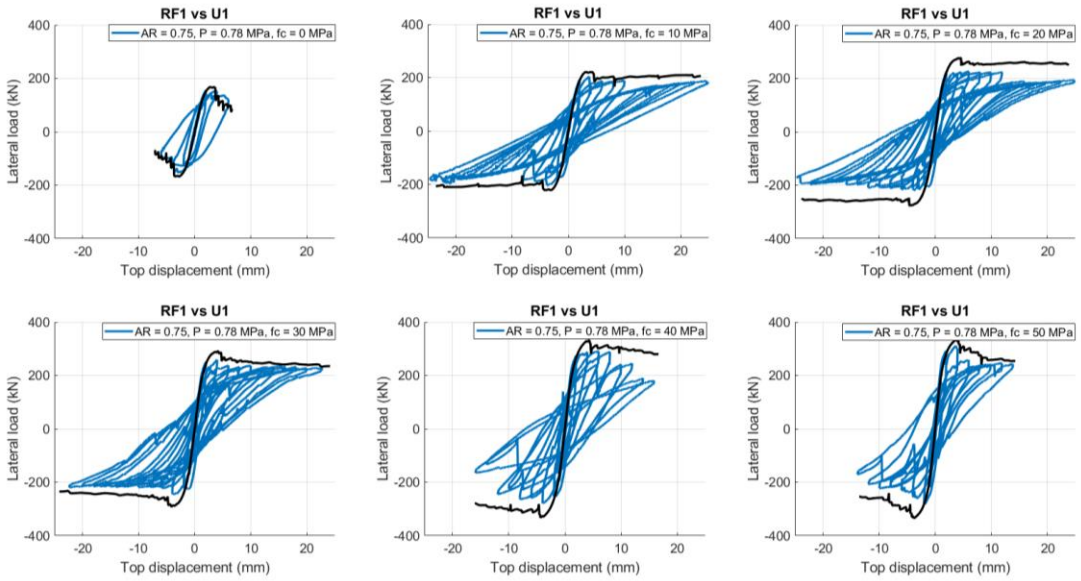

Figure 4.6. Global response of ECC retrofitted masonry wall with ECC compressive strength 0, 10, 20, 30, 40, 50 MPa under 0.78 MPa vertical pressure for aspect ratio 0.75.

The global behavior of the walls with a wall aspect ratio of 0.75 under 0.78 MPa pressure is illustrated in Figure 4.6. The same trend was observed in this case as in the previous case. The strength was 152, 203, 220, 245, 279 and 282 kN for ECC fc 0, 10, 20, 30, 40 and 50 MPa. 33% strength increase with the addition of low-strength ECC. Aspect ratio 0.75 resulted in less strength than aspect ratio 0.5 under the same vertical pressure loading, but higher strength than the previous vertical pressures applied to this aspect ratio. Moreover, the black pushover curves differ in peak strength and ultimate strength. The cases of 20 MPa and 40 MPa ECC layer cases can be highlighted. One has a difference in peak strength, while the second has a difference in ultimate strength. Monotonic loading may have some uncertainties while investigating the structure elements under seismic loadings.

Figures 4.7-4.9 shows the masonry wall with an aspect ratio of 1.0 unretrofitted and retrofitted with 10, 20, 30, 40, and 50 MPa ECC strength under 0.43, 0.60, and 0.78 MPa pressures.

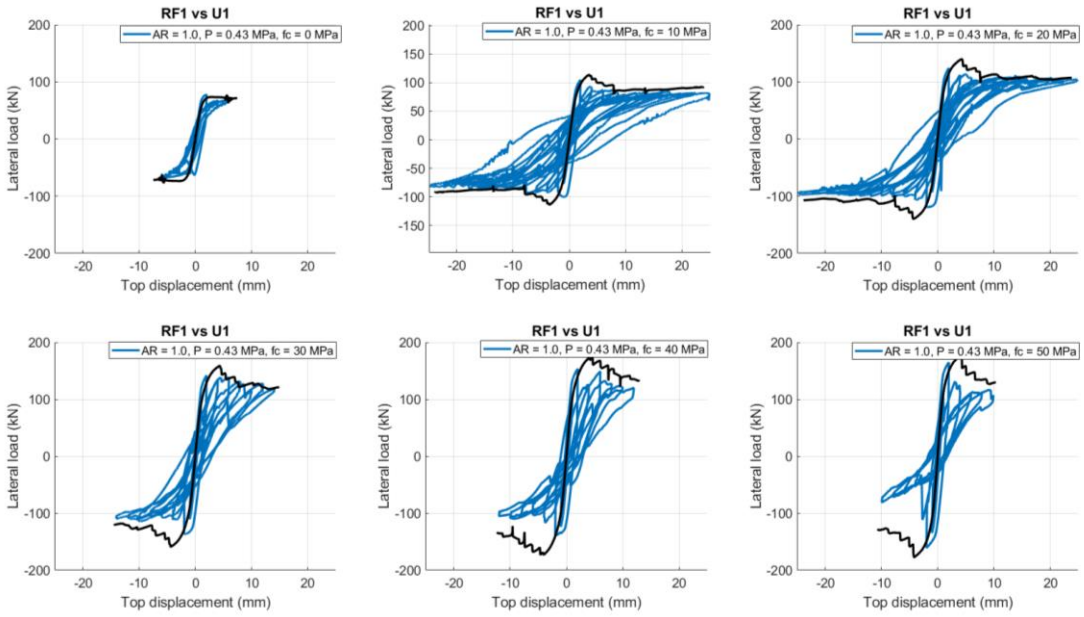

Figure 4.7. Global response of ECC retrofitted masonry wall with ECC compressive strength 0, 10, 20, 30, 40, 50 MPa under 0.43 MPa vertical pressure for aspect ratio 1.0.

It should be noted that, with the increase of the aspect ratio of the wall, the loops are becoming less wide. For instance, loops of aspect ratio 1.0 are narrower rather than 0.75 and 0.5. This implies that it could not cover more strength to widen the loop than the other two. It can also be linked to the failure mode; a clearer conclusion can be drawn after the contour plot study in Chapter 4.2. Figure 4.7 represents the aspect ratio of 1.0 masonry walls under vertical pressure of 0.43 MPa, which are covered with different strength retrofitting composites. Compared to the smaller aspect ratio, the maximum lateral loads are reduced to 74, 100, 119, 137, 140, and 161 kN for the ECC compressive strengths 0, 10, 20, 30, 40, and 50 MPa, respectively. The retrofit to the masonry wall enhanced the poor wall by 35%. Adding the ECC to the high aspect ratio wall enhances the retrofitted wall under the same pressure less than the low aspect ratio wall. For instance, the enhancement percentage for the 0.5 aspect ratio and 0.75 aspect ratio was 44 %, and 36%, respectively, while the wall aspect ratio 1.0 improved by 35 %. Moreover, the behavior of the masonry wall under monotonic loading differs from that of the cyclic loading case, as stated in previous parameter results.

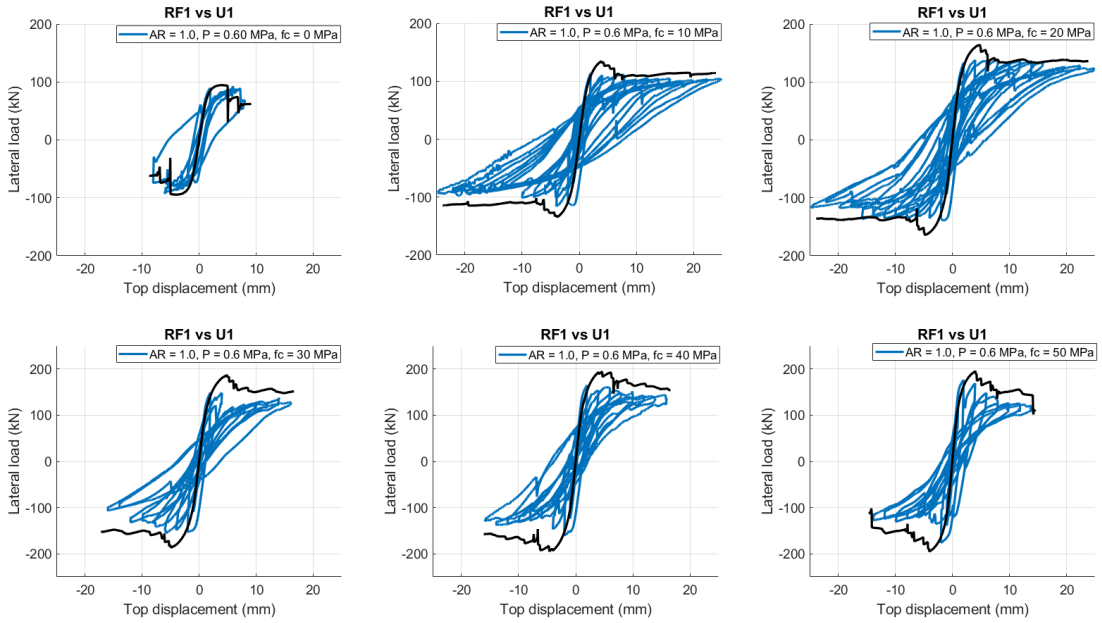

Figure 4.8. Global response of ECC retrofitted masonry wall with ECC compressive strength 0, 10, 20, 30, 40, 50 MPa under 0.60 MPa vertical pressure for aspect ratio 1.0.

The wall with an aspect ratio subjected to the vertical pressure of 0.60 MPa can be observed in Figure 4.8. Unretrofitted masonry wall had 89 kN, while ECC retrofitted wall with composite strength 10, 20, 30, 40, and 50 MPa had 112, 138, 149, 160 and 175 kN wall strength, respectively. The addition of retrofit increased the unretrofitted wall strength by at least 26%. The change in this percentage was noticed to decrease with the increase in vertical pressure and wall aspect ratio. The strength drop of the wall with the increase of ECC strength was less sharp than in other aspect ratios. However, the deformation capacities are lessening with the addition of ECC strength. For example, masonry walls only could withstand up to 8 mm displacement, while ECC retrofitted walls with ECC strength 10, 20, 30, 40, and 50 MPa could withstand 25, 25, 16, 16, and 14 mm displacement. The black line showing the behavior of the wall under monotonic loading for the current parameters was also distinct in strength values from the cyclic one.

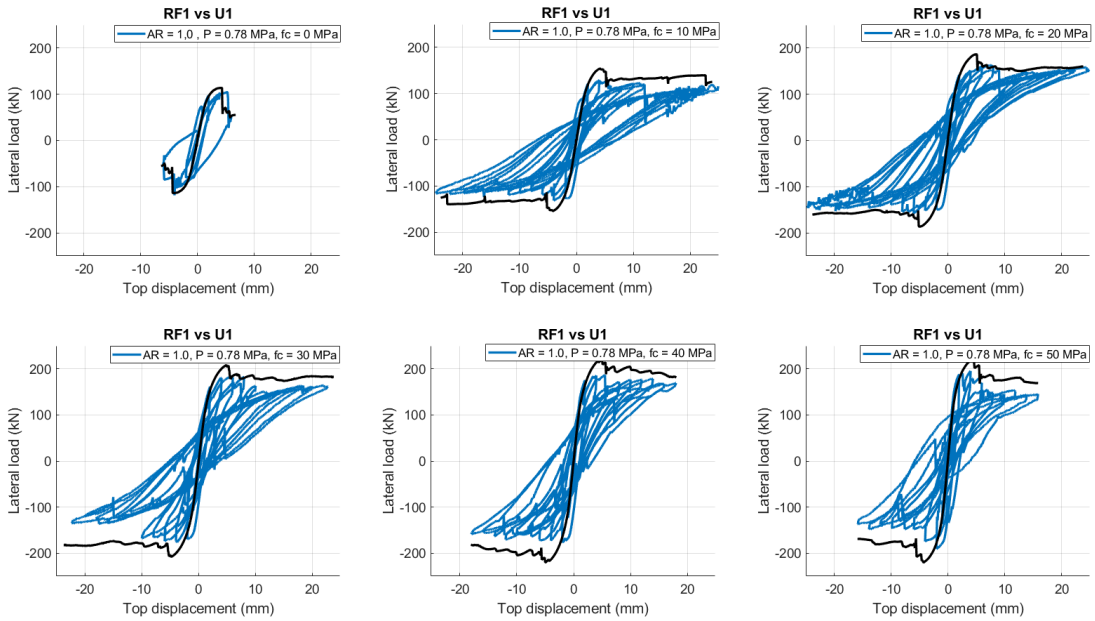

Figure 4.9. Global response of ECC retrofitted masonry wall with ECC compressive strength 0, 10, 20, 30, 40, 50 MPa under 0.78 MPa vertical pressure for aspect ratio 1.0.

For the vertical pressure 0.78 MPa shown in Figure 4.9, the peak strengths were 105, 129, 156, 176, 187, and 191 kN for ECC strength 0, 10, 20, 30, 40 and 50, respectively. The retrofitting approach enhanced the wall to 23% with the lowest 10 MPa retrofit. Strength values were more than other vertical pressures of the same aspect ratio but less than other aspect ratios under the same vertical pressure.

For all cases, the loop widening for the retrofitted walls compared to the unretrofitted wall was common. The depicted hysteresis curves of fc 10 and 20 MPa have negligible strength degradation after reaching the maximum strength due to the rocking at the base of the masonry wall. Moreover, with the increase of vertical pressure and aspect ratio, the addition of retrofit had less minimum effect on the unretrofitted wall strength. Besides the behavior of the wall under cyclic loading, the pushover analysis for all cases is drawn with a black line. As can be seen, the response under monotonic loading contrasts with the cyclic loading response as was assumed. Some of them resulted, in smoother behavior, while the cyclic showed some strength drop, meaning the pushover analysis for the walls subjected to the earthquake, which may occur in a cyclic pattern, is not proper to study.

4.2 Contour plots and failure modes of masonry walls

The deformed shapes of bricks for the wall without ECC and with ECC at specific displacement can be found in this section. The deformed compressive damage contours of masonry for three aspect ratios, under three different vertical pressures are shown in Figure 25-27. Deformed shape contours of unretrofitted walls of all cases are studied, to observe the failure mode modification with the addition of ECC. The damage was evaluated using the equivalent plastic strain (PEEQ) of concrete damaged plasticity material. The deformed shape of masonry and ECC was provided separately, to study the behavior of both components. The tensile equivalent plastic strain of the CDP model was utilized to evaluate the damage of ECC. Figures 4.10-4.12 show the deformed compressive damage contour of masonry with and without ECC under vertical pressure equivalent to 3, 4, and 5 story building at 8 mm displacement for three aspect ratios. The first layer of bricks was considered as elastic material to imitate the fixed foundation of the wall.

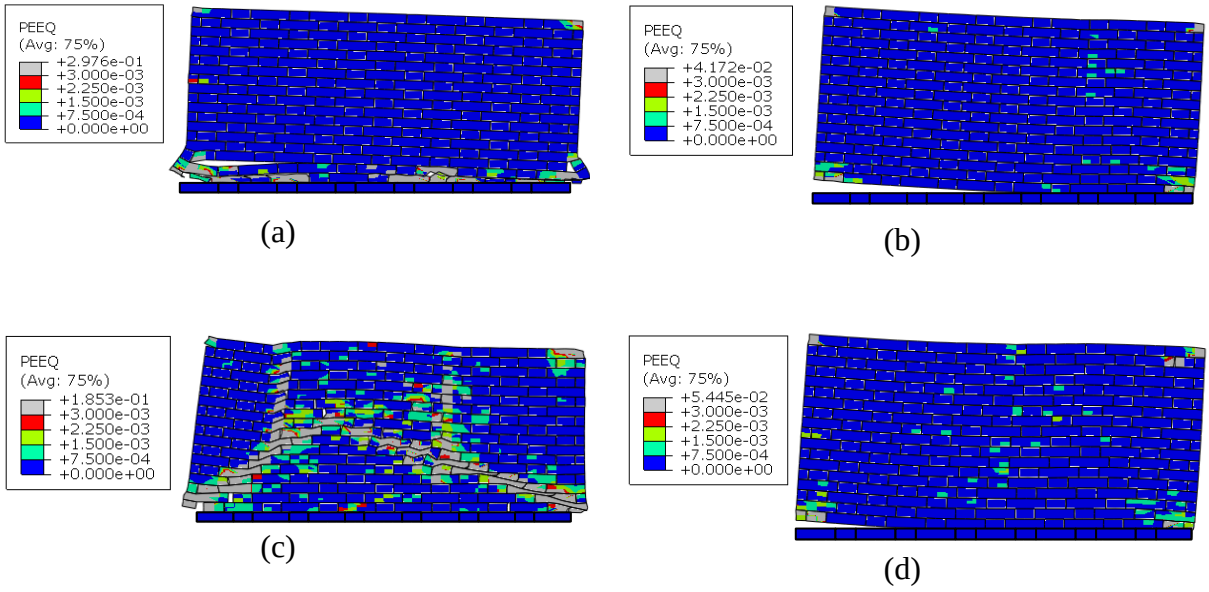

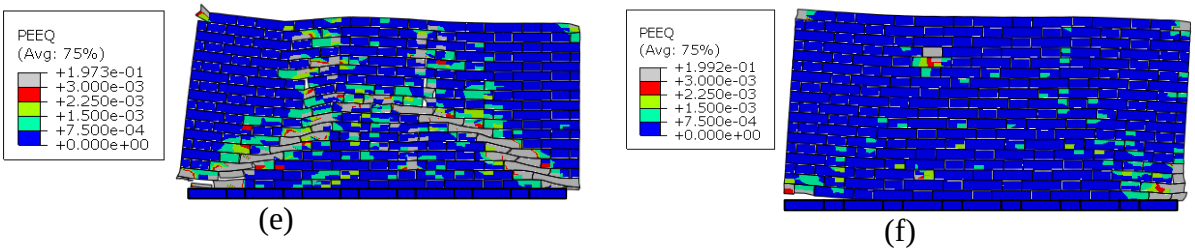

(e) (f)

Figure 4.10. Deformed compressive damage contours of masonry with aspect ratio 0.5 (a) without ECC, (b) with ECC under 0.43 MPa vertical pressure, (c) without ECC, (d) with ECC under 0.60 MPa vertical pressure, (e) without ECC, (f) with ECC under 0.78 MPa vertical pressure.

As can be seen from Figure 4.10a, the unretrofitted wall with an aspect ratio of 0.5 under low axial pressure (0.43 MPa) started with uplifting and experienced sliding of the second layer with the elements of toe crushing. Figure 4.10b clearly demonstrates how the ECC protected the bricks from early-stage damage. Figures 4.10c-d demonstrates the deformed compressive damage contour of masonry walls with and without ECC under vertical pressure equivalent to 4 story building. As for 0.60 MPa vertical pressure (Figures 4.10. c-d), masonry without ECC protection experienced the diagonal shear failure mode as in Figure 2.2a, and ECC in Figure 4.10d, modified this most risky failure mode (Mustafaraj & Yardim, 2019) into rocking failure combined with toe crushing as described in Figure 2.2c-d in Chapter 2.1. Walls under vertical pressure equivalent to the 5 story building (0.78MPa) are shown in Figure 4.10e-f. The same pattern was observed in vertical pressure, 0.60 MPa, and diagonal shear failure swift to the rocking was observed under high pressure, which is 0.78 MPa. As the vertical pressure increases, it increases damage at the toe of the wall.

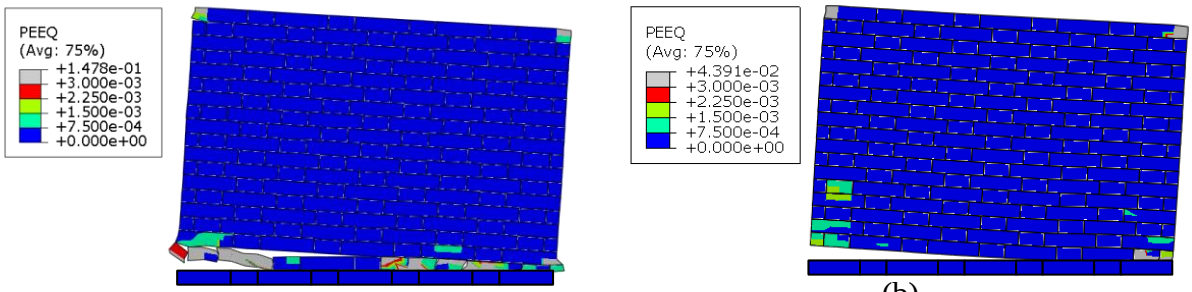

(a) (b)

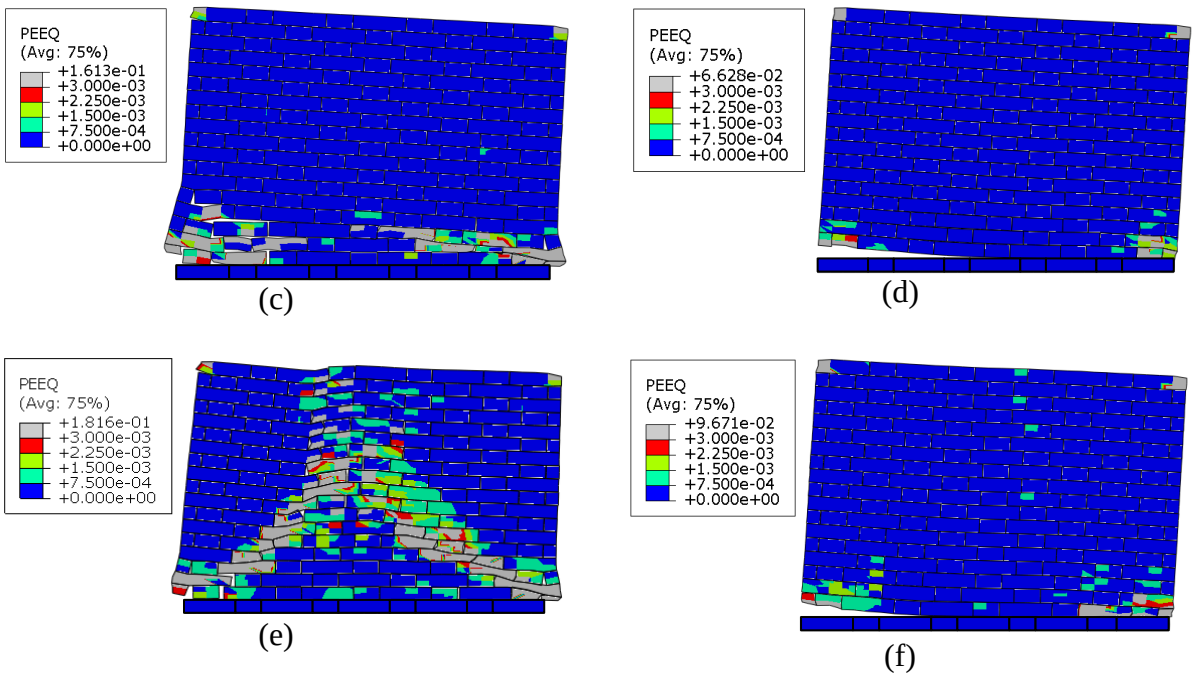

Figure 4.11. Deformed compressive damage contours of masonry with aspect ratio 0.75 (a) without ECC, (b) with ECC under 0.43 MPa vertical pressure, (c) without ECC, (d) with ECC under 0.60 MPa vertical pressure, (e) without ECC, (f) with ECC under 0.78 MPa vertical pressure.

Figure 4.11a-f compare contour plots of masonry walls with and without ECC for different vertical pressures applied at 8 mm displacement. The deformed pattern of the unretrofitted masonry walls with an aspect ratio of 0.75, under low vertical pressure or 0.43 MPa pressure, the wall undergoes light toe crushing failure (Figure 4.11a), subjected to medium vertical pressure or 0.60 MPa experienced toe crushing (Figure 4.11c), while high vertical pressure or 0.78 MPa pressure resulted in diagonal shear failure (Figure 4.11e). However, all three cases were improved with the addition of ECC. They changed their failure modes toe crushing, diagonal shear failure into rocking failure with minor uplift as shown in Figure4.11b, 4.11d, and 4.11f. Rocking failure is the most desired failure mode with minor structural damage after seismic activities.

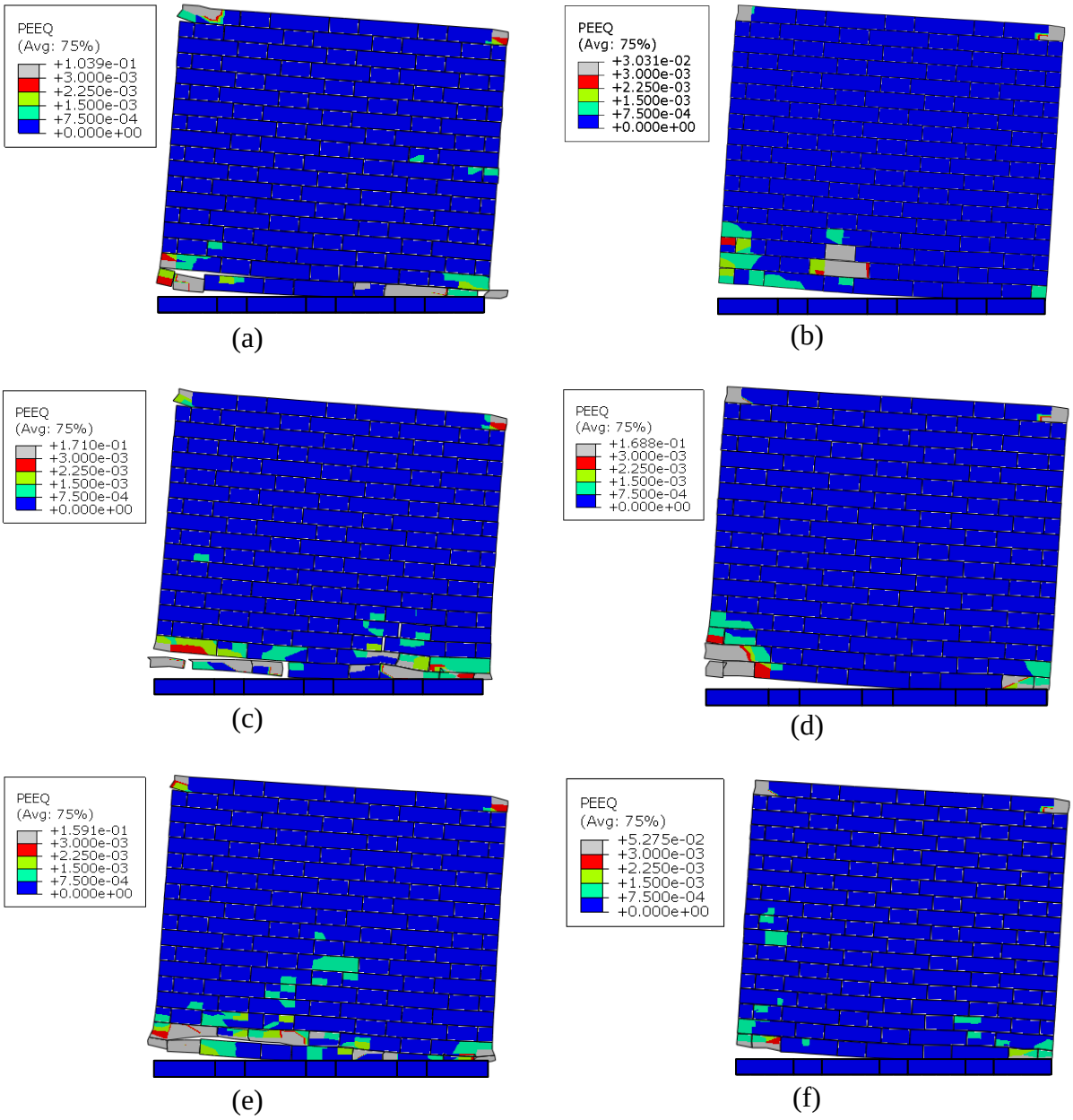

Figure 4.12. Deformed compressive damage contours of masonry with aspect ratio 1.0 (a) without ECC, (b) with ECC under 0.43 MPa vertical pressure, (c) without ECC, (d) with ECC under 0.60 MPa vertical pressure, (e) without ECC, (f) with ECC under 0.78 MPa vertical pressure.

Compared to the previous two aspect ratios, masonry-only wall models with an aspect ratio of 1.0 showed less damaged deformed patterns at 8 mm displacement in Figures 4.12a-f. The masonry walls without an ECC layer under three different vertical pressures damaged the second

layer of bricks. Nevertheless, the ECC also improved these failure modes of masonry walls, enhanced the loose second layer of bricks, and converted the mode into rocking.

Besides the brick's behavior, the ECC deformed contour plots were also investigated, to see the difference in deformed shapes between different strength ECC layers.

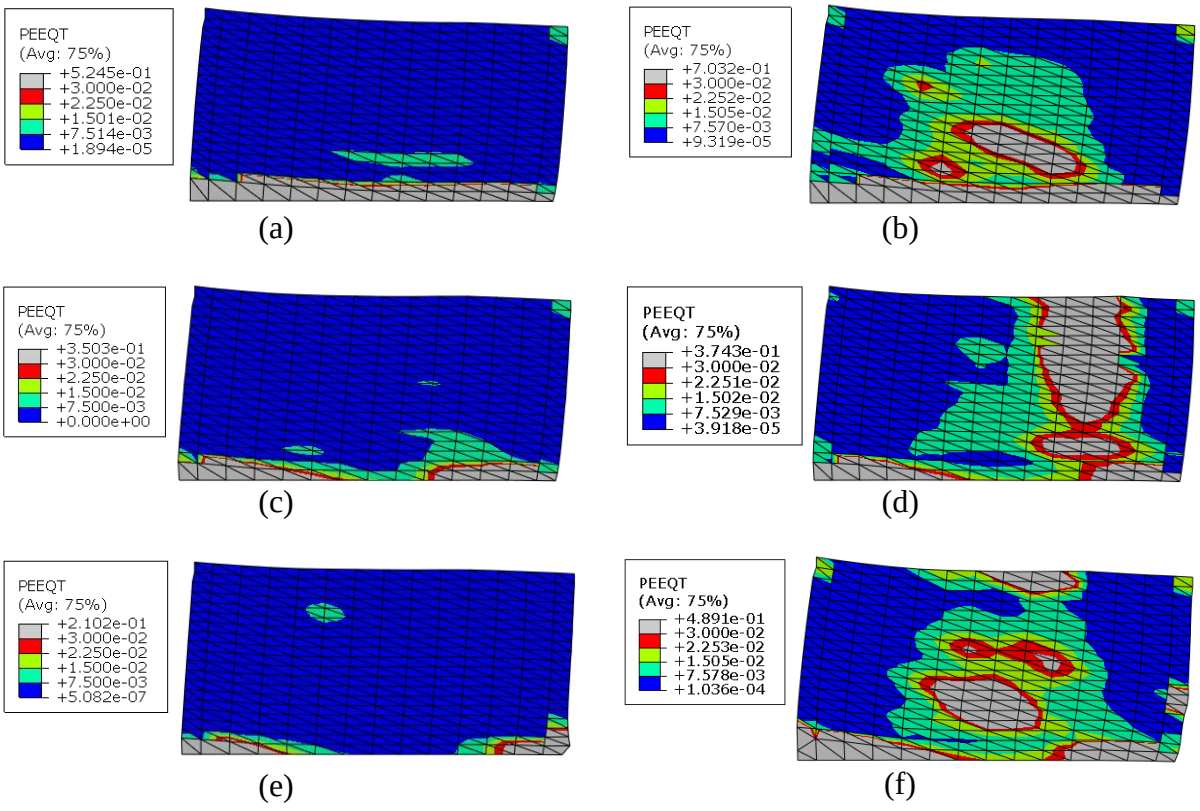

Figure 4.13. Deformed tensile damage contours of ECC with (a) compressive strength 10 MPa and (b) 40 MPa under 0.43 MPa vertical pressure, (c) compressive strength 10 MPa and (d) 40 MPa under 0.60 MPa vertical pressure, (e) compressive strength 20 MPa and (f) 50 MPa under 0.78 MPa vertical pressure on the wall with aspect ratio 0.5.

As for the ECC layer for the wall with an aspect ratio of 0.5, deformed tensile damage contours can be found in Figure 4.13. ECC of walls with low-strength ECC is less damaged and can be found near the bottom of the layer, while normal ECC undergoes more damage along the retrofit layer, reaching the ECC's tensile strain limit. The increasing vertical pressure also influences the damage to the ECC layer.

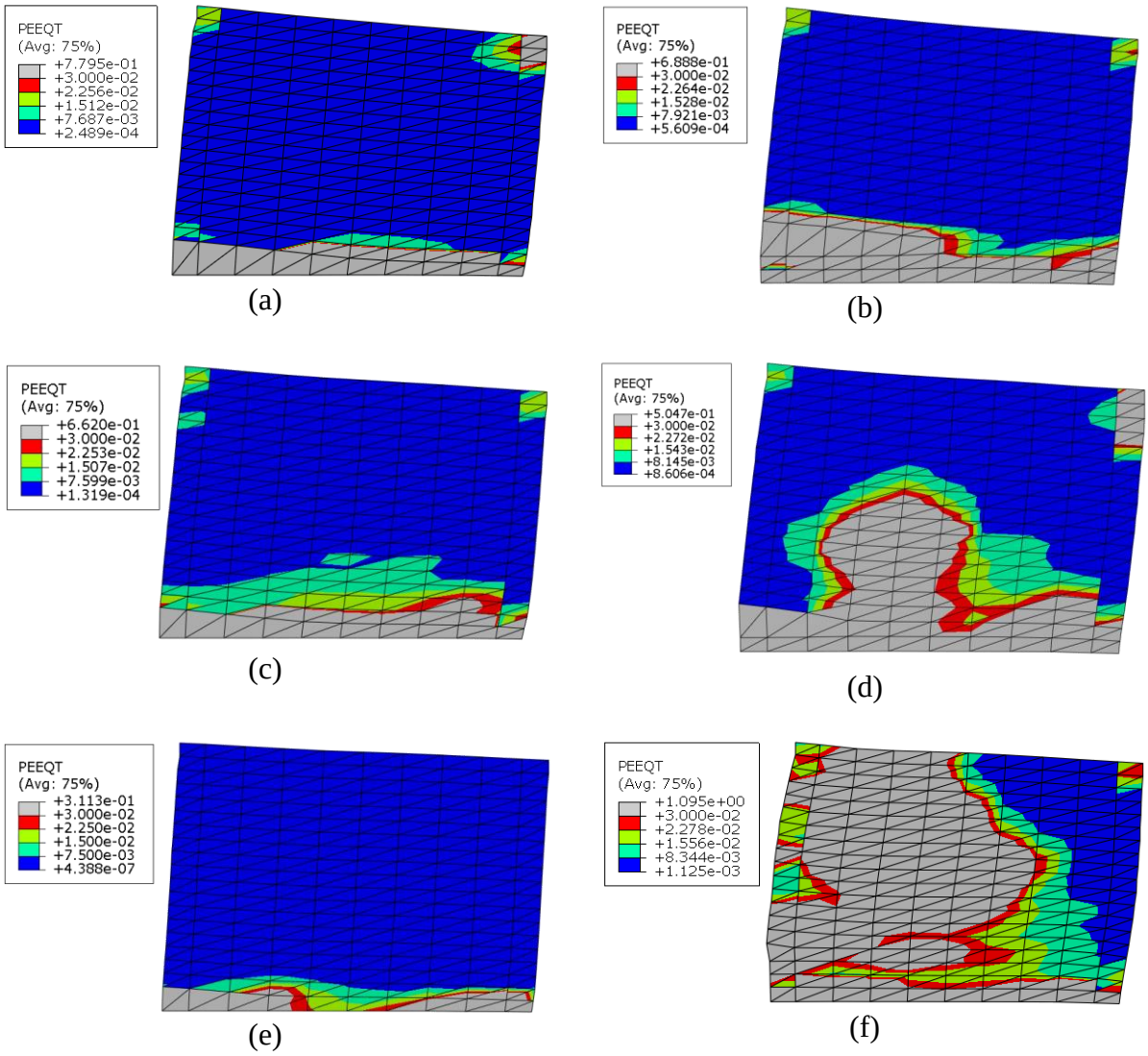

Figure 4.14. Deformed tensile damage contours of ECC with (a) compressive strength 10 MPa and (b) 30 MPa under 0.43 MPa vertical pressure, (c) compressive strength 10 MPa, and (d) 50 MPa under 0.60 MPa vertical pressure, (e) compressive strength 10 MPa and (f) 40 MPa under 0.78 MPa vertical pressure on the wall with aspect ratio 0.75.

Figure 4.14 illustrates the deformed tensile damage plot of the wall aspect ratio of 0.75. It experiences the same pattern as the wall with an aspect ratio of 0.5. The main damaged part of the ECC is the horizontal bottom part for the low-strength ECC. For normal-strength ECC, it is included horizontally at the bottom, and then vertically, it is spread to the upper part of the ECC layer.

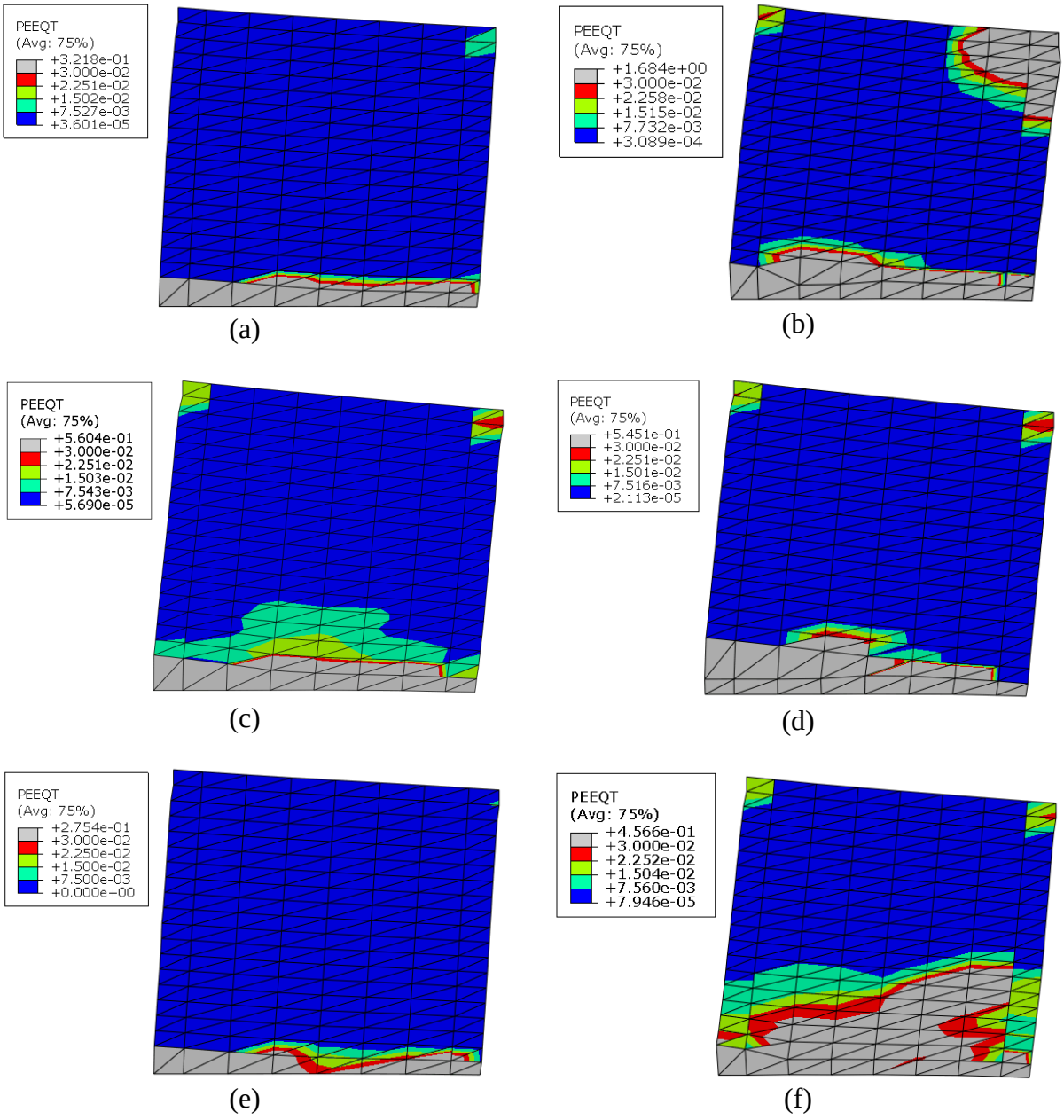

Figure 4.15. Deformed tensile damage contours of ECC with (a) compressive strength 10 MPa and (b) 40 MPa under 0.43 MPa vertical pressure, (c) compressive strength 20 MPa, and (d) 50 MPa under 0.60 MPa vertical pressure, (e) compressive strength 10 MPa and (f) 40 MPa under 0.78 MPa vertical pressure on the wall with aspect ratio 1.0.

Moreover, the deformed shapes of the ECC layer of the wall with an aspect ratio of 1.0 under different vertical pressures are shown in Figure 4.15. The ECC on the wall is covered with a low-strength ECC layer, under three vertical pressures; the most damaged part of the ECC is

bottom levels, the same as in previous wall aspect ratios. In this aspect ratio, for the normal-strength ECC, the damaged layer is expanded or spread to the middle layer and has the top right corner reaching the tensile strain limit of ECC.

4.3 Component results of masonry walls

The lateral behavior of the wall was evaluated with the contribution of each component as masonry cohesion, friction, and ECC. Cohesion and friction component results can be summarized as a single masonry component. These component results will present the contribution to the global response of the wall. Components contribution results can help to observe the trend of lateral load for the ECC and masonry separately. The masonry and ECC component results of walls with different ECC strengths for aspect ratios 0.5, 0.75, and 1.0 under three vertical pressures are presented in Figures 4.16-4.18.

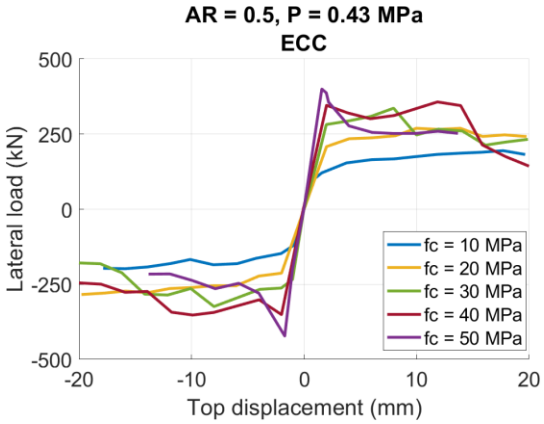

(a)

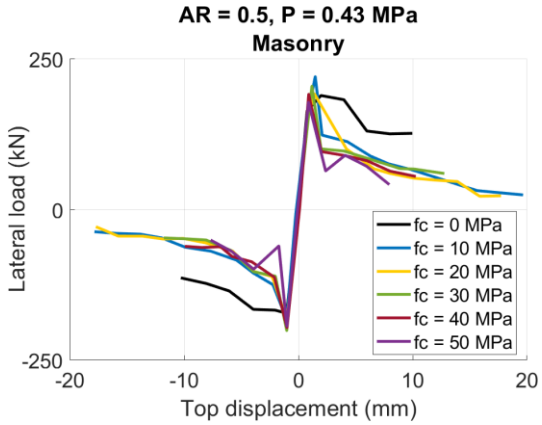

(b)

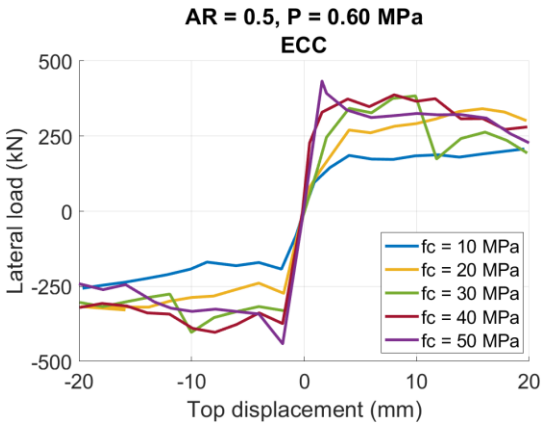

(c)

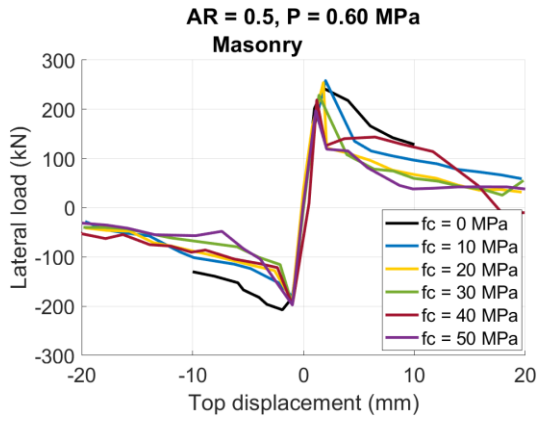

(d)

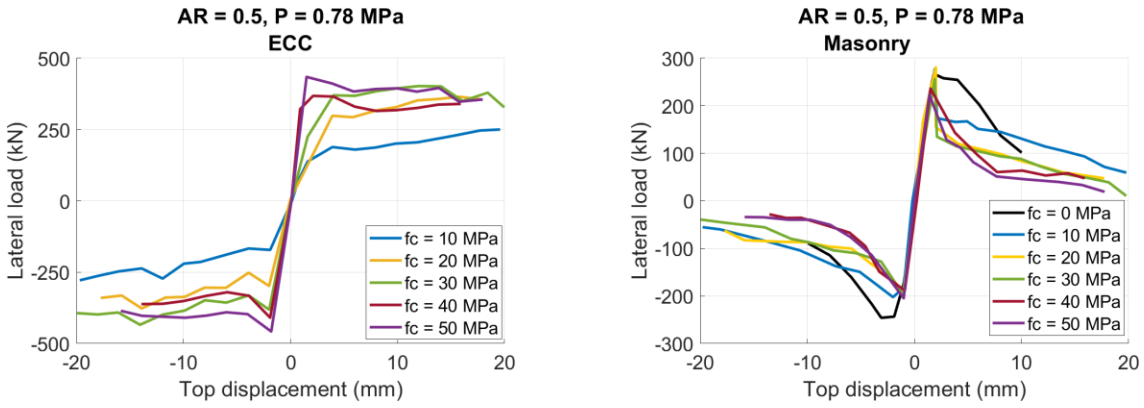

(e) (f)

Figure 4.16. ECC and masonry contribution for the ECC retrofitted walls with aspect ratio 0.5 under vertical pressure (a)-(b) 0.43 MPa, (c)-(d) 0.60 MPa, and (e)-(f) 0.78 MPa.

Figure 4.16 shows the ECC and masonry lateral strengths for the aspect ratio 0.5 under different vertical pressures. Figures 4.16a-b represents the vertical pressure 0.43 MPa, Figures 4.16c-d for 0.60 MPa, and Figures 4.16e-f for 0.78 MPa. Firstly, it is obvious that with the rise of the ECC compressive strength, the lateral load of ECC retrofit increases. As for the masonry component, with the increase of ECC compressive strength, it starts to get reduced. Masonry strength can be absorbed by ECC retrofit. Secondly, ECC for low compressive strengths, 10 MPa to 30 MPa showed smooth lateral load behavior. As for normal-strength ECC, 40 and 50 MPa demonstrate strength drops at failure points.

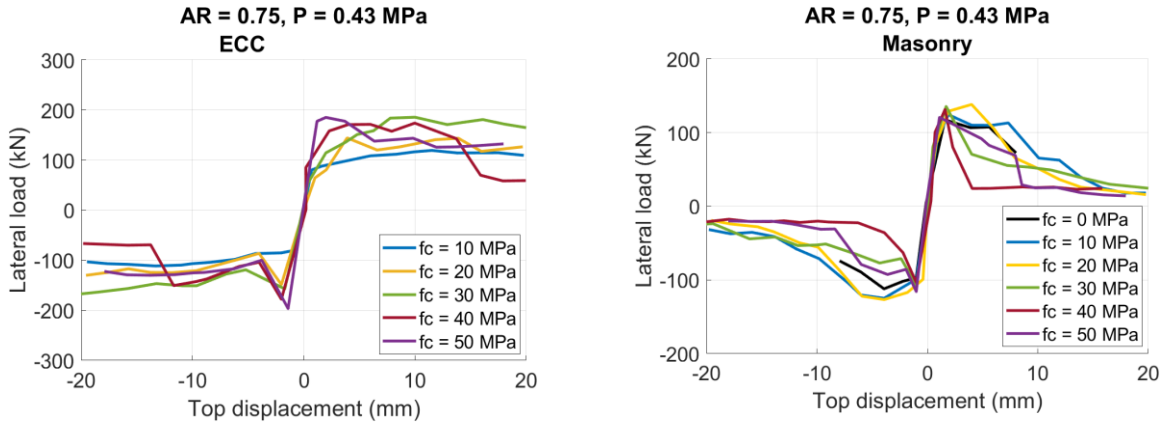

(a) (b)

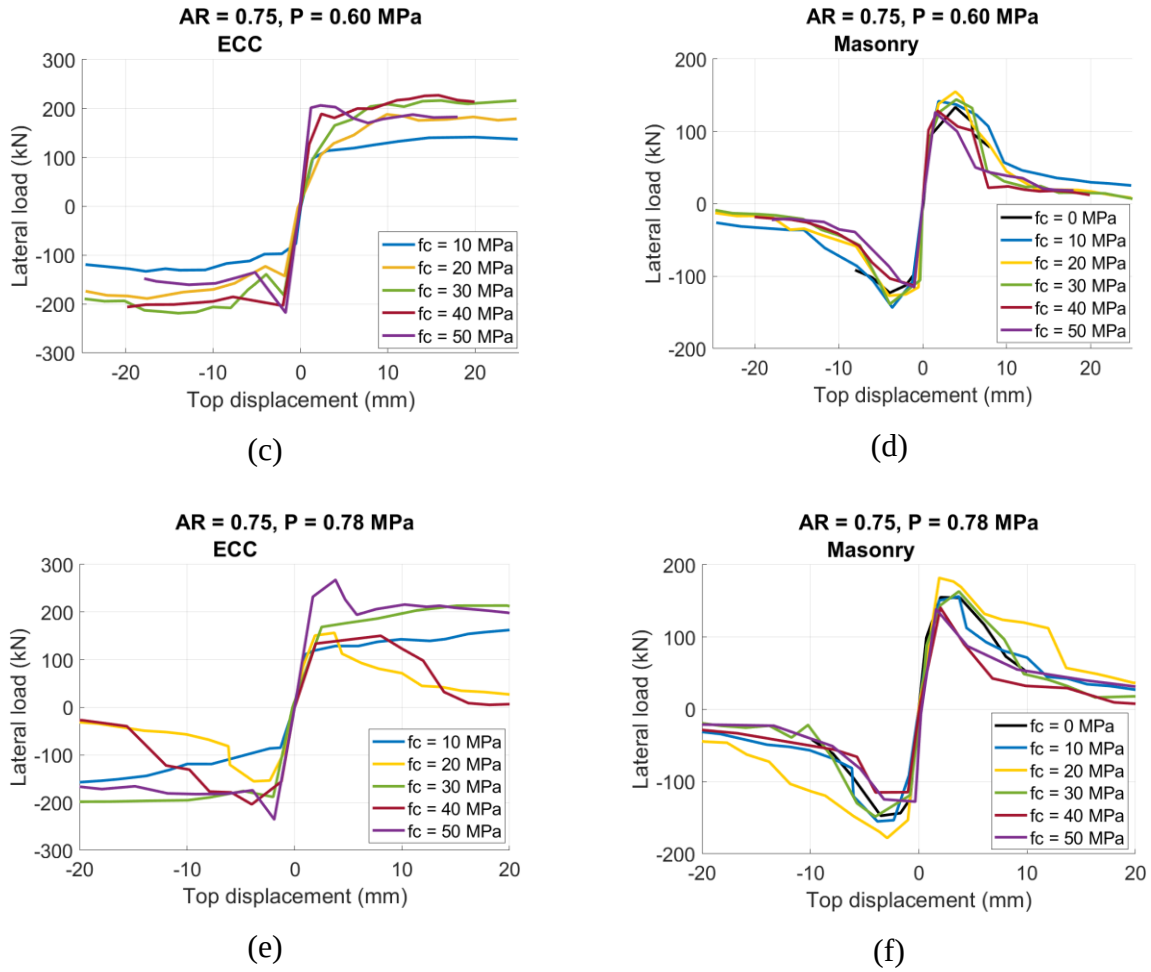

Figure 4.17. ECC and masonry contribution for the ECC retrofitted walls with aspect ratio 0.75 under vertical pressure (a)-(b) 0.43 MPa, (c)-(d) 0.60 MPa, and (e)-(f) 0.78 MPa.

As for the aspect ratio 0.75 case, Figure 4.17 shows the ECC and masonry contribution of the models subjected to the vertical pressure 0.43 MPa (Figures 4.17a-b), 0.60 MPa (Figures 4.17c-d), 0.78 MPa (Figures 4.17e-f). The same ECC lateral load increase and masonry decreases with the ECC compressive strength trend increase, as in aspect ratio of 0.5. In addition, the gradual strength reduction of ECC was observed on 10, 30 MPa ECC retrofit under all three pressures, and 20 MPa under 0.60 MPa, and more strength drop was observed on ECC retrofit with compressive strength 20 MPa under 0.43, 0.78 MPa, and 40, 50 MPa under three different vertical pressure.

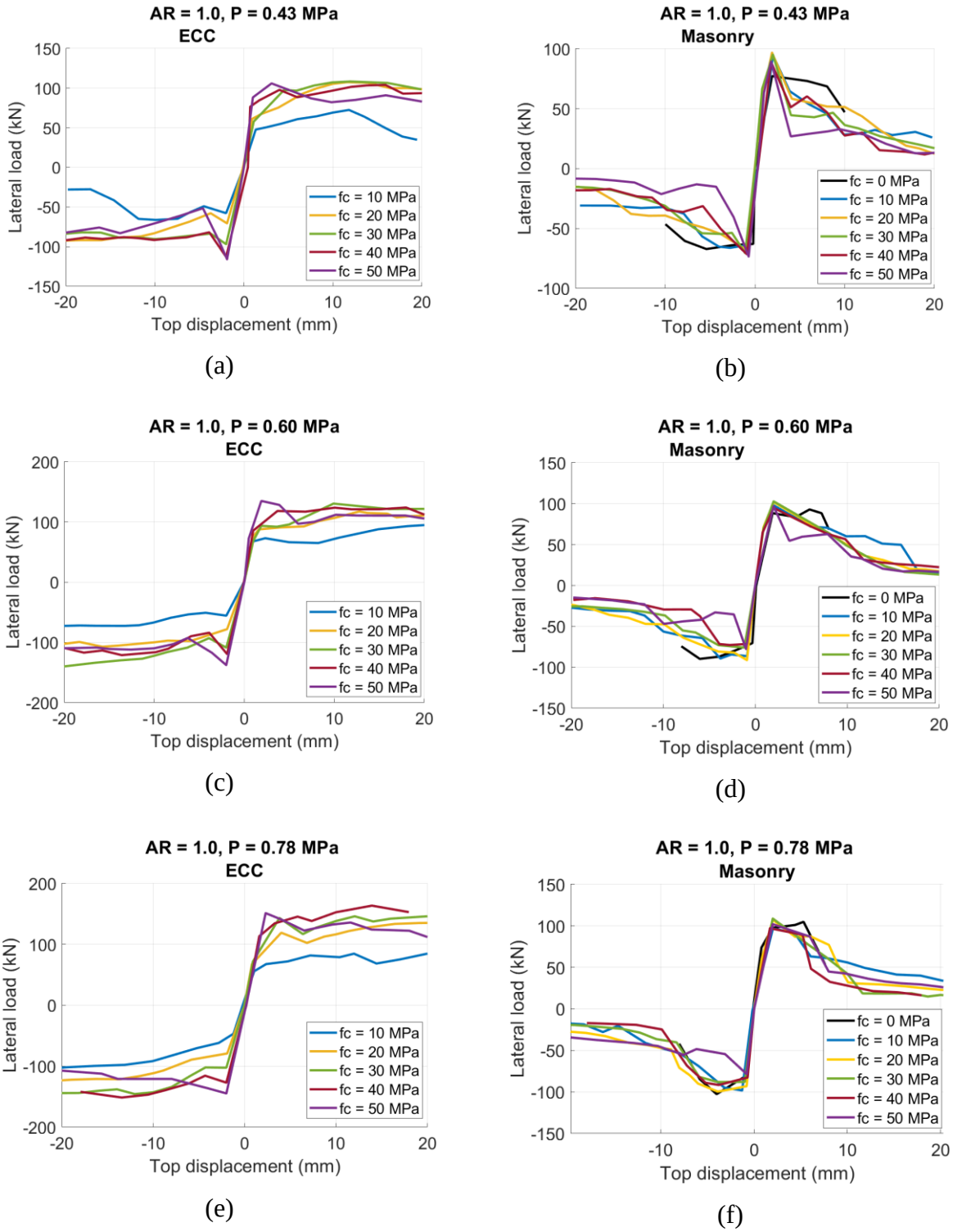

Figure 4.18. ECC and masonry contribution for the ECC retrofitted walls with aspect ratio 1.0 under vertical pressure (a)-(b) 0.43 MPa, (c)-(d) 0.60 MP, and (e)-(f) 0.78 MPa.

Figure 4.18 illustrates the ECC and masonry lateral strengths for the aspect ratio 1.0 under different vertical pressures, 0.43 MPa (Figures 4.18a-b), 0.60 MPa (Figures 4.18c-d), and 0.78 MPa (Figures 4.18e-f). For aspect ratio 1.0, the ECC lateral load increased with increasing ECC compressive strength, and the masonry lateral load decreased. However, compared to aspect ratio of 0.5 and 0.75, aspect ratio of 1.0 cases showed less sharp strength degradation. Moreover, it is noted that with the increasing aspect ratio, and vertical pressure the masonry component results in the curve's peaks getting more rounded and less sharp

4.4 Parametric study results

This part of Chapter 4 elaborates on the impact of study parameters: wall aspect ratio, vertical pressure, and ECC compressive strength on the masonry wall performance. The wall strength, wall stiffness degradation, energy dissipation, wall deformation capacity, and ductility change with the varying study parameters are discussed. Figure 4.19 represents the strength parameters at different loading stages as cracking strength F_{cr} , peak strength F_{max} , and ultimate strength F_u of the wall. These key parameters were obtained from the backbone curves. The minimum absolute value of loading and unloading cases was considered for calculation.

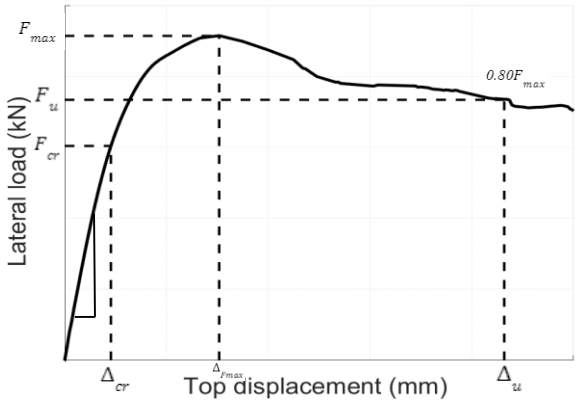

Figure 4.19. Strength and displacement variables at different loading states.

All hysteresis curves shown in Figures 4.1-4.9 represent the displacement capability of the masonry wall corresponding to the 20% maximum strength degradation. The cracking strength of the wall was considered at the first loading stage, which is about 1 mm displacement. 80% of the peak strength was considered as the ultimate strength of the wall. The deformation capacity, Δ_u of the wall is the displacement corresponding to the 20% strength degradation.

Ductility, μ is the ratio of deformation capacity, Δ_u to the displacement corresponding to the cracking strength, Δ_{cr} as presented in Eq. 4.1.

$$\mu = \frac{\Delta_u}{\Delta_{cr}} \tag{4.1}$$

Energy dissipation of each cycle of hysteresis loops is defined as the enclosed area of the loop as shown in Figure 4.20.

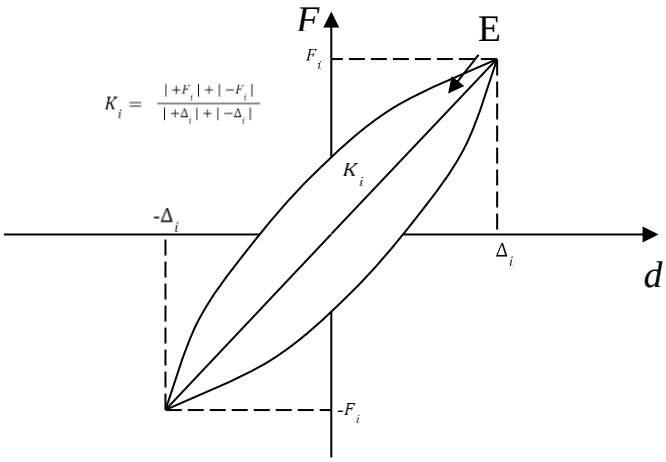

Figure 4.20. Schematic diagram on the definition of energy dissipation

4.4.1 Wall strength

According to the global results provided in Figures 4.1-4.9, the maximum lateral load strengths of the models are summarized in Figures 4.21.

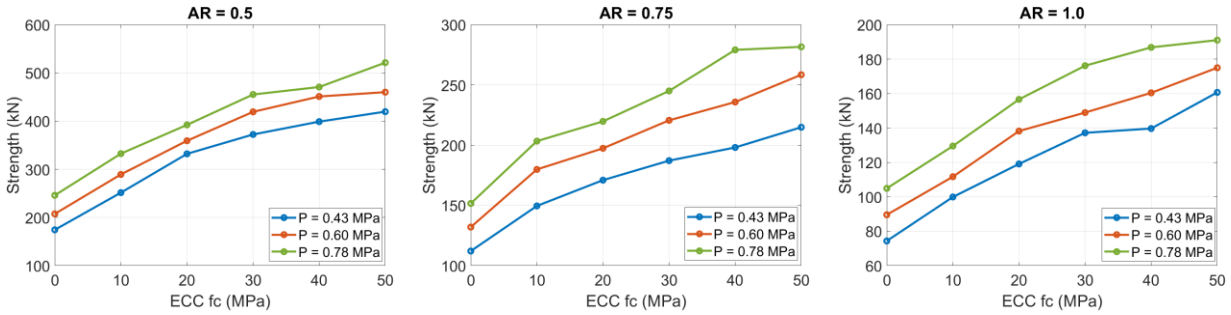

(a) (b) (c)

Figure 4.21. Minimum F_{max} (kN) of loading and unloading cases versus ECC compressive strength (MPa) for vertical pressure 0.43, 0.60, 0.78 MPa for wall aspect ratio (a) 0.5, (b) 0.75, (c) 1.0.

It is obvious that with the rise of vertical pressure, the strength of the wall rises. Moreover, the graphs represent the strength change with the increase of compressive strength of ECC. Normal-strength ECC enhances the lateral load strength of URM walls, rather than low-strength ECC. However, besides the strength, the ductility and deformation capacity are crucial wall behaviors to withstand seismic activities. Thus, the deformation capacity of the walls was investigated for the walls retrofitted with different compressive strengths of ECC, subjected to different vertical pressures. The deformation capacity of the walls is determined at a lateral load corresponding to 80% of peak strength. At the displacement value when the model diverges it is assumed that strength drops straight to zero.

4.4.2 Stiffness degradation

The stiffness degradation was examined by estimating the secant stiffness based on the following expression:

$$K_i = \frac{|+F_i| + |-F_i|}{|+\Delta_i| + |-\Delta_i|} \tag{4.2}$$

, where $\pm F_i$ is the positive and negative peak forces, and $\pm \Delta_i$ is the corresponding displacements for the peak forces, i is the loop number.

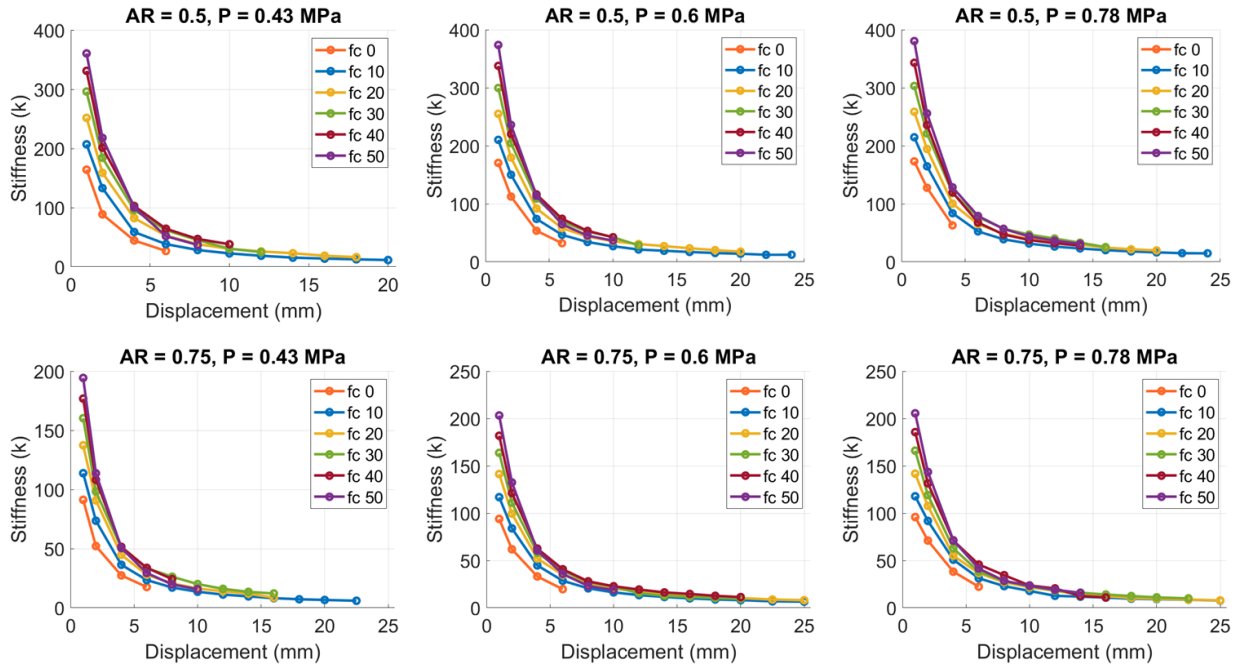

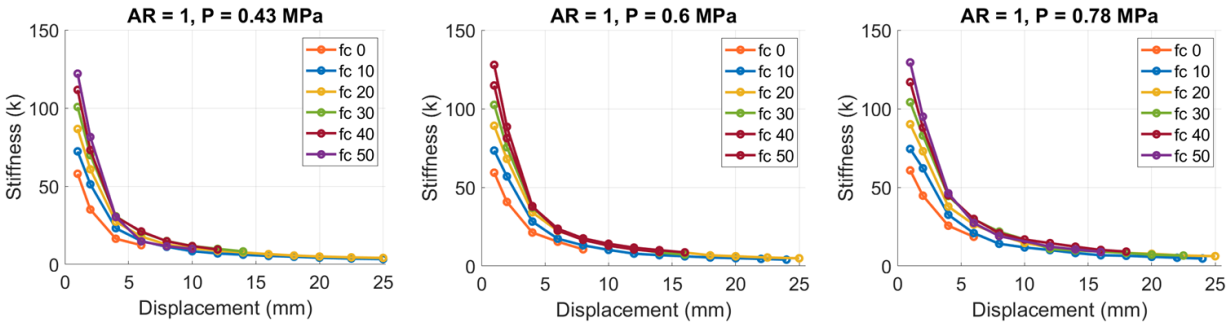

Figure 4.22. The secant stiffness degradation curves for all cases.

The stiffness degradation curves are presented in Figure 4.22 for all cases. The overall trends of the secant stiffness were roughly similar for all, except for the maximum displacements. The increase in ECC strength resulted in higher stiffness at the same displacement but with a decrease in deformation capacity. It is obvious that the unretrofitted walls undergo higher stiffness reduction, resulting in the low strain capacity of the wall. The retrofitted walls with low-strength ECC, have low stiffness degradation compared to the unretrofitted walls enhancing the strain capacity of the walls. Moreover, ECC with lower compressive strength has more secant stiffness. In addition, it is noted that as the aspect ratio of the wall gets higher, the stiffness of the wall is reduced. These stiffness degradation analysis results prove that the retrofitting of the wall assists in increasing the strain capacity, and slows down the cracking, and overall damage of the wall.

4.4.3 Energy dissipation

Energy dissipation was calculated using the area of each loop of hysteretic response curves. Figure 4.23 shows the cumulative energy dissipation at each displacement of the wall.

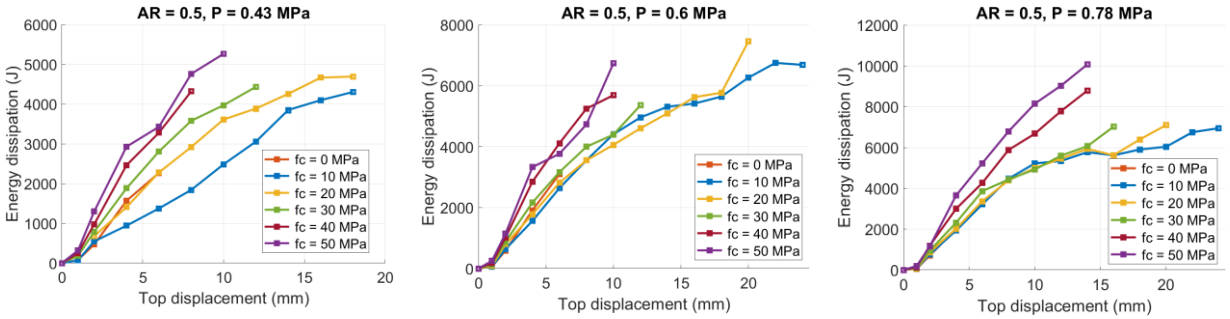

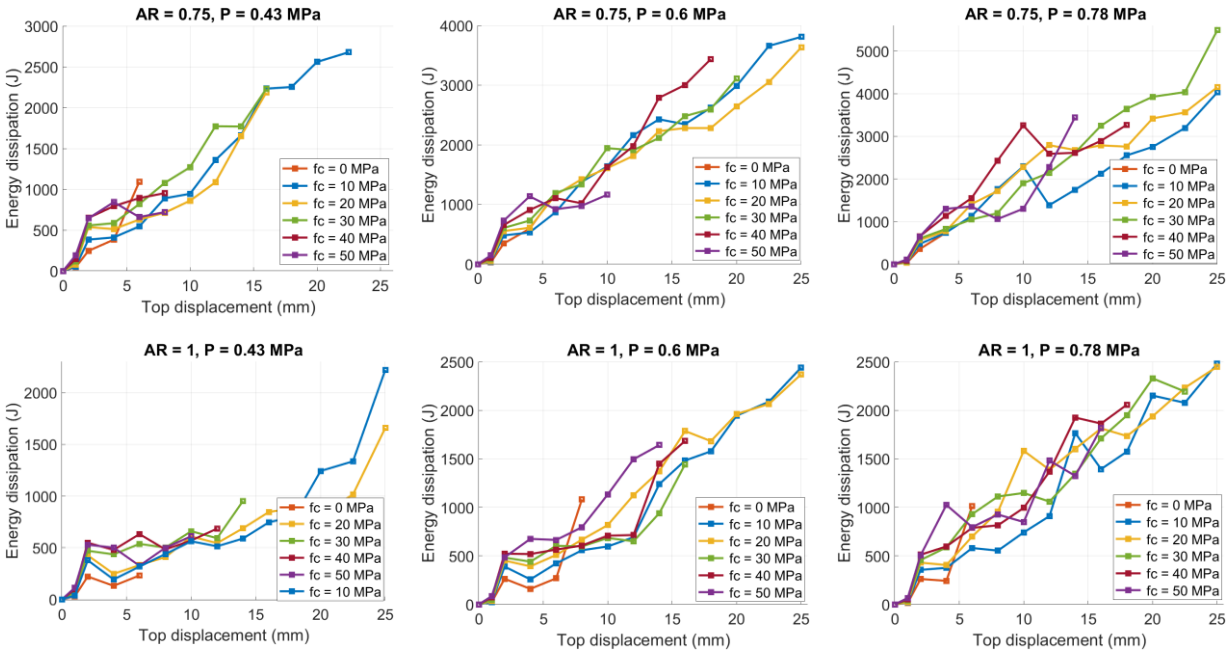

Figure 4.23. Cumulative energy dissipation-displacement curves for all cases.

All curves presented similar energy dissipation at the beginning, 1 mm displacement, then there was an energy dissipation difference between different compressive strengths as can be seen from Figure 4.23. This difference can be due to any significant deformation that occurred during the loading. It is important to note that fc 10 MPa is more tilted to the horizontal axis and experiences low energy dissipation compared to other retrofitted walls at the same displacement. This is because the retrofitting material ECC, is lessening the masonry wall's contribution. To summarize the total cumulative energy dissipation, Figure 4.24 was introduced.

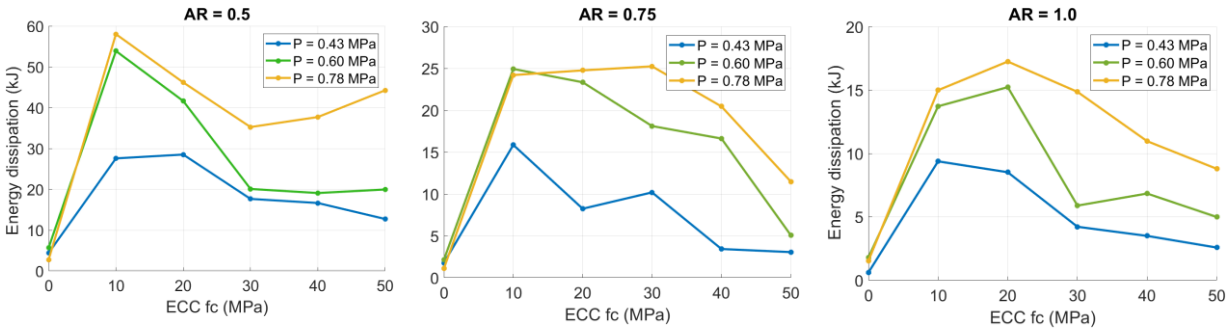

Figure 4.24. Total cumulative energy dissipation-displacement curves for all cases.

For all vertical pressure and aspect ratio cases, the low strength ECC cases with compressive strengths 10, 20 the energy dissipation is highest, in some cases 30 MPa also. They obtained maximum improvement in total cumulative energy dissipation, as shown in Figure 4.24. The strengthening of the wall with an aspect ratio of 0.5, under low pressure, enhances total energy dissipation at most 6.3 times, under 0.60 MPa 9.52 times and under high pressure 21 times. As for the aspect ratio of 0.75, it is 8.96, 11.6, and 22.5 times, and for the aspect ratio of 1.0, it is 6.1, 8.5, and 25 times, respectively.

4.4.4 Wall deformation capacity

In order to inhibit the damage rate of the structure subjected to cyclic seismic activities, it is necessary to have higher deformation capacity and ductility. Thus, these values of the walls were evaluated.

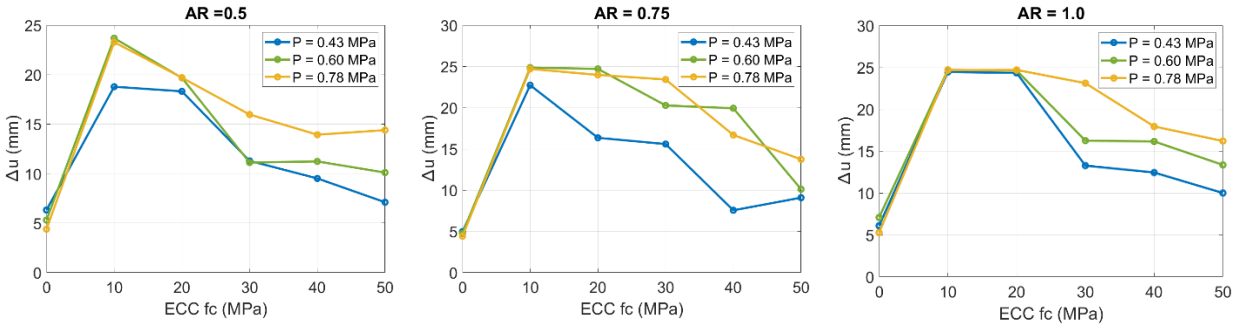

Figure 4.25. Minimum deformation capacity of the walls with aspect ratio 0.5, 0.75, and 1.0 for loading and unloading cases versus ECC compressive strength (MPa) under vertical pressures 0.43, 0.60, 0.78 MPa.

According to the results in Figure 4.25, the overall trend shows that the deformation capacity of the wall decreases with the increase of ECC compressive strength. As it was suggested, the masonry wall was supposed to reach a high deformation capacity with the compressive strength of retrofitting material matching the strength and stiffness of the master masonry wall. In addition, with the increase of vertical pressure, the deformation capacity increased. Walls subjected to 0.60 and 0.78 MPa result show more deformation capacity rather than low vertical pressure applied (0.43 MPa). As for wall aspect ratios, all three values indicated a similar pattern. The low-strength ECC retrofitted walls reach 20 to 25 mm, while normal-strength ECC retrofitted walls fail at an early stage. Moreover, it is noticeable that under high pressure, the deformation capacities of the wall with ECC retrofit 10, 20, and 30 MPa strength barely differ from each other compared to the

former pressures. For the low and moderate vertical pressures, the deformation capacity mainly ECC compressive strength 10 MPa or 20 MPa strength are more distinct than 30, 40, and 50 MPa.

4.4.5 Wall ductility

Figure 4.26 shows the ductility of the masonry walls with aspect ratios 0.5, 0.75, 1.0 under 0.43, 0.60, 0.78 MPa vertical pressure retrofitted with 10,20,30,40,50 MPa ECC compressive strength, and including bare walls. The trend of wall ductility was consistent with the deformation capacity of the wall in Figure 4.25.

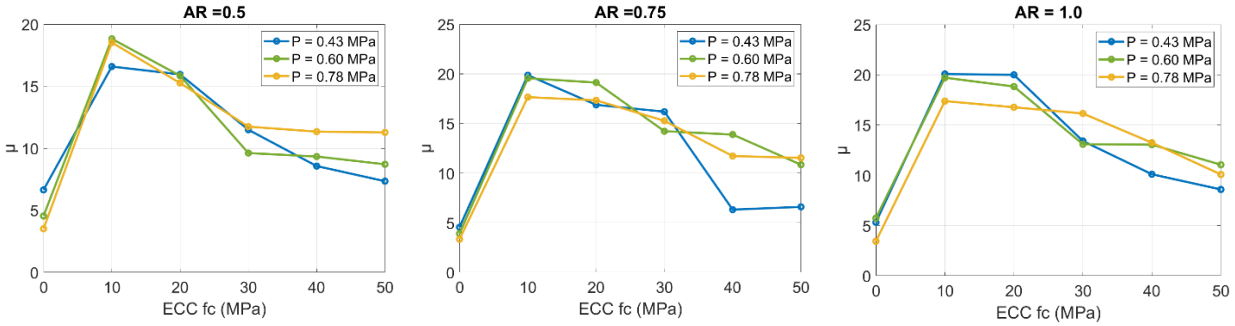

Figure 4.26. Ductility of the walls with aspect ratio 0.5, 0.75, and 1.0 for loading and unloading cases versus ECC compressive strength (MPa) under vertical pressures 0.43, 0.60, 0.78 MPa.

It is obvious that the masonry wall with ECC layer strength 10 MPa showed the highest ductility value, with all proposed wall ratios and vertical pressure. Among wall aspect ratio 0.5, under moderate vertical pressure 0.60 MPa, with ECC retrofit 10 MPa showed the highest ductility rather than the remaining two pressures. The ductility of the wall retrofitted with low-strength ECC was 4.2 times higher than the unretrofitted wall. The retrofitted wall value was 18.8, while the retrofitted 4.5. As for the aspect ratio of 0.75, the masonry wall under 0.43 MPa low pressure with ECC layer 10 MPa demonstrated the highest value, resulting in 19.9, improved by the bare value 4.5, higher to 4.4 times. Among aspect ratio 1.0, under vertical pressure 0.43 MPa, with ECC retrofit 10 MPa was leading with value 20, increasing the ductility from 5.3 of the wall without ECC. Ductility for higher pressure cases of aspect ratios 0.75 and 1.0, with ECC compressive strength 10 MPa and 20 MPa very close to each other, and for aspect ratio 1.0 under all pressures, these two values were also almost similar. Despite that, ECC with a compressive strength of 10 MPa resulted in more wall ductility compared to other ECC compressive strengths.

Chapter 5. Conclusions

5.1 Concluding remarks

Most of the studies of URM walls investigated normal strength ECC which significantly strengthened the unreinforced masonry wall; however, it did not affect the ductility of the wall. That is because of the difference in strength between masonry and ECC. Thus, low-strength ECC is expected to improve the ductility of the wall under cyclic loading. So, low-strength ECC retrofitted masonry walls are expected to have relatively higher ductility rather than walls with normal-strength ECC. This research project can assist in defining the best design parameters for ECC. The 2D analytical model of an unreinforced masonry wall with and without ECC was built in software. In a parametric study, changing ECC strength, the wall's height-to-width ratio, and vertical pressure will help to analyze their effect on the behavior of unreinforced masonry walls under cyclic seismic forces. According to the results, the proposed study can help solve the issue of existing numerous unreinforced masonry buildings in Central Asian countries. The conclusions drawn from this numerical study are as follows:

1) The application of ECC retrofit effectively improves the lateral in-plane behavior of masonry walls, including wall strength, stiffness degradation, energy dissipation, deformation capacity, and ductility.
2) The low-strength ECC retrofit showed higher deformation capacity and ductile behavior, concluding that with the increase of ECC compressive strength, the deformation capacity, and ductility of the wall decreased.
3) The strength and stiffness of the masonry walls increase with the increase of vertical pressure and increase of ECC retrofit compressive strength. Increase in vertical pressure mainly resulted better deformation capacity, but ductility showed inconsistent results with the deformation capacity for higher aspect ratios. However, increase in ECC compressive strength reduces the deformation capacity as well as ductility of the wall.
4) The low-strength ECC shows a lower strength reduction compared to the normal ECC, which possesses poor deformation capacity and ductility abilities.
5) The strength and stiffness of the masonry wall reduce with the increase of wall aspect ratio.

6) The addition of the ECC layer contributes to changing the failure mode from diagonal shear failure mode, and toe crushing failure into rocking failure, which is a more ductile failure mode.
7) There is a difference between the responses of the masonry wall under cyclic and monotonic loading. Cyclic loading shows faster strength degradation than monotonic loading due to cumulative damages.

5.2 Recommendations and future work

In further study, it would be better to improve the stiffness of the calibrated wall model, to reach more accurate results from the parametric study. Experimental verification can be done for the low-strength ECC, since this study was done on normal-strength ECC. Moreover, the two-dimensional model can be converted to a three-dimensional model, to meet the actual geometry of the wall, and to study the behavior of the wall subjected to out-of-plane loading. In this study, the 2D model was utilized due to the time limits since it preserves more time than the 3D model. Structural models subjected to dynamic loadings can also be investigated to understand building behavior during an earthquake. As for the parametric study, more parameters such as ECC thickness, other wall geometries, ECC material properties, brick orders, and out-of-plane loading can be studied in the future, to have a more comprehensive study. Moreover, nowadays plenty of reinforcing composites are introduced to research. Thus, other materials such as basalt textile reinforced mortar composite, sprayed mortar, ferrocement, textile reinforced mortar and steel reinforced grout can also be investigated using the unreinforced masonry wall models.

References

ABAQUS (2010) Analysis User's Manual (Version 6.6.) Providence, RI:Dassaults Systems SIMULIA Corporation.

Abrams, D., & Lynch, J. (2001). Flexural behaviour of retrofitted masonry piers. In *Proceedings of the KEERC-MAE Joint Seminar on Risk Mitigation for Regions of Moderate Seismicity*. Illinois, USA.

Abdulla, K., Cunningham, L., & Gillie, M. (2017). Simulating masonry wall behavior using a simplified micro-model approach. *Engineering Structures, 151*, 349-365. doi: 10.1016/j.engstruct.2017.08.021

Alcaino, P., & Santa-Maria, H. (2008). Experimental Response of Externally Retrofitted Masonry Walls Subjected to Shear Loading. *Journal Of Composites For Construction*, *12*(5), 489-498. doi: 10.1061/(asce)1090-0268(2008)12:5(489)

Amey, R., Elliott, J., Hussain, E., Walker, R., Pagani, M., & Silva, V. et al. (2021). Significant Seismic Risk Potential From Buried Faults Beneath Almaty City, Kazakhstan, Revealed From High-Resolution Satellite DEMs. *Earth And Space Science*, *8*(9). doi: 10.1029/2021ea001664

Babaeidarabad, S., Arboleda, D., Loreto, G., & Nanni, A. (2014). Shear strengthening of un-reinforced concrete masonry walls with fabric-reinforced-cementitious-matrix. *Construction and Building Materials*, *65*, 243–253. https://doi.org/10.1016/j.conbuildmat.2014.04.116

Cakir, F., Uckan, E., Shen, J., Seker, B., & Akbas, B. (2015). Seismic damage evaluation of historical structures during Van earthquake, October 23, 2011. *Engineering Failure Analysis*, *58*, 249-266. doi: 10.1016/j.engfailanal.2015.08.030

Choi, H., Quan, C., & Jin, K. (2023). Nonlinear performance curve estimation of unreinforced masonry walls subjected to in-plane rocking behavior. *Applied Sciences*, *13*(12), 7298. https://doi.org/10.3390/app13127298

Deng, M., & Yang, S. (2018). Cyclic testing of unreinforced masonry walls retrofitted with engineered cementitious composites. *Construction And Building Materials*, *177*, 395-408. doi: 10.1016/j.conbuildmat.2018.05.132

Deng, M., & Yang, S. (2020). Experimental and numerical evaluation of confined masonry walls retrofitted with engineered cementitious composites. *Engineering Structures*, *207*, 110249. https://doi.org/10.1016/j.engstruct.2020.110249

Doran, B., Karslioglu, M., Unsal Aslan, Z., & Vatansever, C. (2022). Experimental and numerical investigation of unreinforced masonry walls with and without opening. *International Journal of Architectural Heritage*, *17*(11), 1833–1854. https://doi.org/10.1080/15583058.2022.2080611

ElGawady, M., Lestuzzi, P., & Badoux, M. (2004). A review of conventional seismic retrofitting techniques for URM. In *13th International Brick and Block Masonry Conference*. Amsterdam.

ElGawady, M., Lestuzzi, P., & Badoux, M. (2006). Retrofitting of masonry walls using shotcrete. In *Proceedings of the NZSEE Conference*. New Zealand.

Hendry, E. A. W. (2001). Masonry walls: Materials and construction. *Construction and Building Materials*, *15*(8), 323–330. https://doi.org/10.1016/s0950-0618(01)00019-8

Hu, Y., Ma, P., & Yao, J. (2023). Effects of aspect ratios and vertical loads on in-plane seismic behavior of unreinforced masonry walls: A numerical simulation. *PLOS ONE*, *18*(3). https://doi.org/10.1371/journal.pone.0282430

Huang, X., Ranade, R., Zhang, Q., Ni, W., & Li, V. C. (2013). Mechanical and thermal properties of green lightweight engineered cementitious composites. *Construction and Building Materials*, *48*, 954–960. https://doi.org/10.1016/j.conbuildmat.2013.07.104

Kadam, S., Singh, Y., & Li, B. (2014). Out-of-plane behaviour of unreinforced masonry

strengthened using ferrocement overlay. *Materials And Structures*, *48*(10), 3187-3203. doi: 10.1617/s11527-014-0390-8

Karantoni, F., & Fardis, M. (1992). Effectiveness of Seismic Strengthening Techniques for Masonry Buildings. *Journal Of Structural Engineering*, *118*(7), 1884-1902. Doi: 10.1061/(asce)0733-9445(1992)118:7(1884)

Kyriakides, M., & Billington, S. (2014). Cyclic Response of Nonductile Reinforced Concrete Frames with Unreinforced Masonry Infills Retrofitted with Engineered Cementitious Composites. *Journal Of Structural Engineering*, *140*(2). doi: 10.1061/(asce)st.1943-541x.0000833

Lourenço, P. B., Rots, J. G., & Blaauwendraad, J. (1994). Assessment of a strategy for the detailed analysis of masonry structures. *DIANA Computational Mechanics '84*, 359–369. https://doi.org/10.1007/978-94-011-1046-4_34

Magenes, G., & Calvi, G. M. (1997). In-plane seismic response of brick masonry walls. *Earthquake Engineering & Structural Dynamics*, *26*(11), 1091–1112. https://doi.org/10.1002/(sici)1096-9845(199711)26:11<1091::aid-eqe693>3.0.co;26

Mustafaraj, E., & Yardim, Y. (2019). Retrofitting damaged unreinforced masonry using external shear strengthening techniques. *Journal of Building Engineering*, *26*, 100913. https://doi.org/10.1016/j.jobe.2019.100913

Niasar, A. N., Alaee, F. J., & Zamani, S. M. (2020). Experimental investigation on the performance of unreinforced masonry wall, retrofitted using engineered cementitious composites. *Construction and Building Materials*, *239*, 117788. https://doi.org/10.1016/j.conbuildmat.2019.117788

Overseas Development Institute. (2016). *Earthquake science and hazard in Central Asia* (pp. 8-11). London: Earthquakes without frontiers.

OYO International. (2009). *The study on earthquake disaster risk management for Almaty City in the Republic of Kazakhstan* (pp. 18-20). Estimated damage and risk mapping.

Pareek, K., Shahnawaz Ansari, M., Saha, P., & Verma, S. (2016). Seismic retrofitting of the structure:an overview. Retrieved 17 December 2016, from https://www.researchgate.net/publication/331982934_SEISMIC_RETROFITTING_OF THE_STRUCTURE_AN_OVERVIEW

Proença, J., Gago, A., & Vilas Boas, A. (2018). Structural window frame for in-plane seismic strengthening of masonry wall buildings. *International Journal Of Architectural Heritage*, *13*(1), 98-113. doi: 10.1080/15583058.2018.1497234

Sailauova, D. (2022). Effect of strength and stiffness of engineered cementitious composites on seismic performance of unreinforced masonry wall.

Shrive, N. G. (2006). The use of fibre reinforced polymers to improve seismic resistance of masonry. *Construction and Building Materials*, *20*(4), 269–277. https://doi.org/10.1016/j.conbuildmat.2005.08.030

Singh, M., Saini, B., & Chalak, H. (2019). Performance and composition analysis of engineered cementitious composite (ECC) – A review. *Journal Of Building Engineering*, *26*, 100851. doi: 10.1016/j.jobe.2019.100851

Türkmen, S., De Vries, B. T., Wijte, S. N., & Vermeltfoort, A. T. (2019). In-plane behaviour of clay brick masonry wallettes retrofitted with single-sided fabric-reinforced cementitious matrix and deep mounted carbon fibre strips. *Bulletin of Earthquake Engineering*, *18*(2), 725–765. https://doi.org/10.1007/s10518-019-00596-2

Vanin, A., & Foraboschi, P. (2012). In-plane behavior of perforated brick masonry walls. *Materials and Structures*, *45*(7), 1019–1034. https://doi.org/10.1617/s11527-011-9814-x

Vasconcelos, G., & Lourenço, P. B. (2009). In-plane experimental behavior of stone masonry walls under cyclic loading. *Journal of Structural Engineering*, *135*(10), 1269–1277. https://doi.org/10.1061/(asce)st.1943-541x.0000053

Vintzileou, E., Mouzakis, C., Adami, C.-E., & Karapitta, L. (2015). Seismic behavior of three-leaf stone masonry buildings before and after interventions: Shaking table tests on a two-storey masonry model. *Bulletin of Earthquake Engineering*, *13*(10), 3107–3133. https://doi.org/10.1007/s10518-015-9746-x

Wang, S., & Li, V. (2003). Lightweight engineered cementitious composites (ECC). In PRO 30: *4th international RILEM workshop on high performance fiber reinforced cement composites (HPFRCC 4)* (Vol. 1, p. 379). Michigan: RILEM Publications.

Wieland, M., Pittore, M., Parolai, S., Begaliev, U., Yasunov, P., & Tyagunov, S. et al. (2014). A Multiscale Exposure Model for Seismic Risk Assessment in Central Asia. *Seismological Research Letters*, *86*(1), 210-222. doi: 10.1785/0220140130

Zeng, B., Li, Y., & Cruz Noguez, C. (2021). Modeling and parameter importance investigation for simulating in-plane and out-of-plane behaviors of unreinforced masonry walls. *Engineering Structures*, *248,* 113233. doi: 10.1016/j.engstruct.2021.113233